Universitat de Barcelona

Master in Astrophysics, Particle Physics and Cosmology

Master Thesis

Neutrino oscillations and CP violation: analysis of NOνA data

Author:
Iván Esteban Muñoz

Supervisor:
Mª Concepción González García

29th June 2016

Universitat de Barcelona

Abstract

This work represents the initiation of the author into research in the phenomenology of neutrino oscillations in the present experimental context. As a start, the formalism and most important aspects of neutrino oscillation phenomenology are reviewed in Chapter 1. Additionally, a brief overview of the different experiments that have led to the current global picture is presented, giving particular attention to accelerator neutrino experiments.

The original part of this work focuses on the analysis of the results from the NOνA experiment, the latest in the neutrino oscillation experimental programme, with the aim of quantifying their impact in the present understanding of neutrino oscillation parameters. Specifically, Chapter 2 contains the details of a "simulation" developed to replicate the analyses of the different NOνA data samples. Chapter 3 describes its impact on a global fit. In particular, the NOνA data sample with highest statistics modifies the preferred neutrino mass ordering from normal to inverted, favours $\theta_{23} > 45°$, and increases the statistical confidence on the CP violating phase δ_{CP}, confirming the hint $\delta_{\text{CP}} \sim \frac{3\pi}{2}$. The resulting global fit including the results of this work has been made publicly available [1].

Finally, a dedicated analysis of the current statistical confidence on leptonic CP violation and the neutrino mass ordering has been carried out, with the goal of addressing deviations from Gaussianity and the dependence on the θ_{23} octant. The study, described in Chapter 3, uses data from most modern accelerator neutrino experiments (NOνA, T2K and MINOS) and considers statistical aspects via a Monte Carlo simulation. As a result, at present CP conservation (i.e., $\delta_{\text{CP}} = 0, 2\pi$) is only disfavoured at about 1σ, while $\delta_{\text{CP}} \in [0.16\pi, 0.84\pi]$ is disfavoured with a 90% CL for any value of θ_{23}. Besides, the inverted mass ordering is disfavoured with a 90% CL for $\delta_{\text{CP}} \lesssim \pi$ and any value of θ_{23}.

The analyses and methodology employed in this work will be updated once more data becomes available in early July. That new data should have the potential to significantly tighten the presented bounds.

Contents

Chapter 1

Overview of neutrino physics

I have done a terrible thing, I have postulated a particle that cannot be detected.
— Wolfgang Pauli

Neutrinos are among the most elusive elementary particles we have detected. First proposed by Wolfgang Pauli to account for energy conservation in nuclear beta decays [2], they currently are an essential part of the Standard Model of Particle Physics (SM) as the weak isospin partners of the charged leptons. Nevertheless, some of their properties, in particular whether CP symmetry is violated in the leptonic sector, are still poorly known [3]. Because of that, there is currently a strong theoretical [4, 5] and experimental [6, 7] work towards the determination of this and related properties.

One of the main reasons for the relatively limited experimental knowledge on neutrino physics is their low interaction cross section: the penetrating power in solid matter of neutrinos emitted in beta decay is around 10^4 light years [8]. Therefore, it was 26 years after their existence was proposed that neutrinos were first directly observed in an underground experiment carried out by C.L. Cowan and F. Reines [9]. Remarkable experimental advances, however, have allowed to build sophisticated detectors that have opened a new precision era in neutrino physics [10–16].

1.1 Introducing massive neutrinos

Originally, in the SM neutrinos were introduced minimally, just to explain their interactions: due to the chiral structure of the SM, only left handed neutrinos were required. Since no gauge-invariant, renormalisable operator exists giving neutrinos a mass without introducing new fields, in the SM neutrinos are strictly massless [17][1]. Furthermore, the best experimental constraints on the neutrino mass scale set it below the eV scale [18].

Nevertheless, in order to explain a deficit in the observed Solar neutrino flux, it was proposed to introduce small neutrino masses that would cause flavour-oscillations similar to the ones in the quark sector [19]. As will be seen in Sec. 1.2, there is now plenty of evidence that neutrinos have masses and, therefore, that the SM should be extended. The minimal form of such extensions is discussed below.

1.1.1 Lagrangian for massive neutrinos

As has been mentioned, from the theoretical point of view neutrino masses require to introduce new degrees of freedom in the SM. The simplest option, that does not introduce additional interactions, is to identify those new degrees of freedom with right-handed particles with no weak hypercharge, what are commonly known as sterile neutrinos. The most general gauge invariant renormalisable Lagrangian one can add to the SM is then

$$-\mathcal{L}_{M_\nu} = Y_{ij}\bar{\nu}_{si}\tilde{\phi}^\dagger L_{Lj} + \frac{1}{2}M_{N_{ij}}\bar{\nu}_{si}\nu^c_{sj} + \text{h.c.}\,. \tag{1.1}$$

[1] Unless otherwise specified, most of the information in this chapter has been extracted from Ref. [17]

$\nu_{si}\,,\ i \in \{1,\dots,m\}$ are m sterile neutrinos, $L_{Lj}\,,\ j \in \{1,2,3\}$ are the SM lepton doublets, $\tilde{\phi}^\dagger = (i\tau_2\phi^*)^\dagger$ with ϕ the SM Higgs , and $\nu^c \equiv C\bar{\nu}^T = -i\gamma^2\gamma^0\bar{\nu}^T$ is the charge conjugated field of ν. Y and $M_N = M_N^T$ are complex $m\times 3$ and $m\times m$ matrices, respectively.

After electroweak spontaneous symmetry breaking, the first term in Eq. (1.1) generates at low energy what is known as a Dirac mass term,

$$M_{D_{ij}}\bar{\nu}_{si}\nu_{Lj}\,, \tag{1.2}$$

with $M_{D_{ij}} = Y_{ij}\frac{v}{\sqrt{2}}$, being v the vacuum expectation value of the Higgs field. This term is similar to the one present for the charged fermions, and with no additional operators gives neutrinos a mass $\sim M_D$.

The second term in Eq. (1.1), however, is more interesting. It has the structure of a Majorana mass term, violating any U(1) charge carried by ν_s; in particular it breaks lepton number L by two units if L is assigned to ν_s as to make the Dirac mass term L conserving.

The diagonalisation of the whole Lagrangian (1.1) leads to $3+m$ mass eigenstates ν_M that are Majorana fermions, i.e., $\nu_M^c = \nu_M$. These eigenstates describe free neutrino propagation. In what refers to the eigenvalues, two interesting cases can be distinguished:

- $M_N = 0$: this option is equivalent to imposing *by hand* lepton number conservation in any theory embedding the SM (otherwise, even if $M_N = 0$ at tree level, loop corrections from new physics could induce $M_N \neq 0$ [20]). It allows to rearrange, for $m = 3$, the 6 Majorana eigenstates in 3 Dirac fermions. In this case, there is no natural explanation for the lightness of neutrinos, which would require $Y \lesssim 10^{-11}$.
- $M_N \gg M_D$: this is expected in SM extensions such as SO(10) GUTs [21–23] or left-right symmetric models [24]. In this case, the diagonalisation leads to 3 light eigenstates of masses $\sim M_D^2/M_N$, which are mostly left-handed, and m heavy eigenstates of masses $\sim M_N$, which are mostly right-handed. This naturally explains the lightness of neutrinos through what is known as the *see-saw mechanism*: the heavier are the heavy states, the lighter are the light ones.

There is also an alternative, model-independent approach to neutrino masses. If the SM is considered as an effective theory valid up to some scale $\Lambda_{\rm NP}$, higher dimensional non renormalisable effective operators built with the SM fields and respecting the SM gauge symmetry will effectively appear in the Lagrangian at low energy, suppressed by different powers of $1/\Lambda_{\rm NP}$. Interestingly, the lowest order (least suppressed) effective operator that only contains SM fields and is consistent with gauge symmetry is

$$\mathcal{O} = \frac{Z^\nu_{ij}}{\Lambda_{\rm NP}}\left(\bar{L}_{Li}\tilde{\phi}\right)\left(\tilde{\phi}^T\bar{L}^c_{Lj}\right) + \text{h.c.}\,. \tag{1.3}$$

After spontaneous symmetry breaking, this term leads to

$$\mathcal{O} = \frac{Z^\nu_{ij}}{2}\frac{v^2}{\Lambda_{\rm NP}}\bar{\nu}_{Li}\nu^c_{Lj} + \text{h.c.}\,, \tag{1.4}$$

a Majorana mass term for neutrinos. The diagonalisation of Z^ν_{ij} yields 3 Majorana mass eigenstates whose mass is suppressed by $\Lambda_{\rm NP}$, i.e., the lightness of neutrinos is naturally explained by the large value of $\Lambda_{\rm NP}$. Indeed, if the Lagrangian (1.1) with $M_N \gg M_D$ is considered, integrating out the heavy eigenstates leads to a Lagrangian of the form (1.4) with $\Lambda_{\rm NP} \sim M_N$.

1.1.2 Charged current interaction Lagrangian

Besides the mass Lagrangian (1.1), the charged current Lagrangian gets also modified by introducing neutrino masses, leading to flavour mixing as in the quark sector. For $3+m \equiv n$ neutrino mass eigenstates, in the mass basis this Lagrangian reads

$$-\mathcal{L}_{CC} = \frac{g}{\sqrt{2}}\begin{pmatrix}\bar{e}_L & \bar{\mu}_L & \bar{\tau}_L\end{pmatrix}U^{\rm lep}\begin{pmatrix}\nu_{M1}\\ \nu_{M2}\\ \nu_{M3}\\ \vdots\\ \nu_{Mn}\end{pmatrix}W^+_\mu - \text{h.c.}\,, \tag{1.5}$$

where ν_i , $i \in \{1, \ldots, n\}$ are the neutrino mass eigenstates and U^{lep} is a $3 \times n$ matrix verifying

$$U^{\text{lep}} U^{\text{lep}\dagger} = I_{3\times 3} \,. \tag{1.6}$$

If there is no new interactions for the charged leptons, U^{lep} can be identified as a $3 \times n$ submatrix of an $n \times n$ matrix V^{ν} relating neutrino flavour and mass eigenstates. In particular, for the Lagrangian (1.1):

$$\begin{pmatrix} \nu_{L1} \\ \nu_{L2} \\ \nu_{L3} \\ \nu^c_{s1} \\ \vdots \\ \nu^c_{sm} \end{pmatrix} = V^{\nu} L \begin{pmatrix} \nu_{M1} \\ \nu_{M2} \\ \nu_{M3} \\ \vdots \\ \nu_{Mn} \end{pmatrix} , \tag{1.7}$$

with L the left-handed projector.

If there is only three light Majorana neutrinos, U^{lep} is a 3×3 unitary matrix usually referred to as the PMNS matrix [18]. Using three angles $\theta_{12}, \theta_{13}, \theta_{23} \in [0, 90°]$ and three phases $\delta_{\text{CP}}, \eta_1, \eta_2 \in [0, 2\pi]$, it can be conveniently parametrised as

$$\begin{aligned} U^{\text{lep}} &= \begin{pmatrix} 1 & 0 & 0 \\ 0 & c_{23} & s_{23} \\ 0 & -s_{23} & c_{23} \end{pmatrix} \begin{pmatrix} c_{13} & 0 & s_{13}e^{-i\delta_{\text{CP}}} \\ 0 & 1 & 0 \\ -s_{13}e^{i\delta_{\text{CP}}} & 0 & c_{13} \end{pmatrix} \begin{pmatrix} c_{12} & s_{12} & 0 \\ -s_{12} & c_{12} & 0 \\ 0 & 0 & 1 \end{pmatrix} \begin{pmatrix} e^{i\eta_1} & 0 & 0 \\ 0 & e^{i\eta_2} & 0 \\ 0 & 0 & 1 \end{pmatrix} \\ &= \begin{pmatrix} c_{12}c_{13} & s_{12}c_{13} & s_{13}e^{-i\delta_{\text{CP}}} \\ -s_{12}c_{23} - c_{12}s_{13}s_{23}e^{i\delta_{\text{CP}}} & c_{12}c_{23} - s_{12}s_{13}s_{23}e^{i\delta_{\text{CP}}} & c_{13}s_{23} \\ s_{12}s_{23} - c_{12}s_{13}c_{23}e^{i\delta_{\text{CP}}} & -c_{12}s_{23} - s_{12}s_{13}c_{23}e^{i\delta_{\text{CP}}} & c_{13}c_{23} \end{pmatrix} \begin{pmatrix} e^{i\eta_1} & 0 & 0 \\ 0 & e^{i\eta_2} & 0 \\ 0 & 0 & 1 \end{pmatrix} , \end{aligned} \tag{1.8}$$

where $c_{ij} \equiv \cos\theta_{ij}$ and $s_{ij} \equiv \sin\theta_{ij}$. Note that, unlike in the parametrisation of the quark CKM mixing matrix, there is two new phases η_1 and η_2. These phases appear due to the Majorana mass term (1.4)$\propto \bar{\nu}\nu^*$: because of it, global phases cannot be absorbed in the neutrino fields.

For three Dirac neutrinos, on the other hand, the parametrisation in Eq. (1.8) still holds with $\eta_1 = \eta_2 = 0$. Finally, for three light and m heavy neutrinos stemming from Lagrangian (1.1), U^{lep} has the form

$$U^{\text{lep}} \simeq \left(\left(1 - \tfrac{1}{2} M_D^{\dagger} M_N^{*-1} M_N^{-1} M_D\right) V_l \quad M_D^{\dagger} M_N^{*-1} V_h \right) , \tag{1.9}$$

where V_l and V_h are 3×3 and $m \times m$ unitary matrices, respectively. Therefore, if only light neutrinos are considered a 3×3 non-unitary mixing matrix is obtained. The unitarity violation, however, is suppressed by a factor $\sim (M_D/M_N)^2$ and can be safely ignored in what follows.

1.1.3 Neutrino oscillations

An immediate phenomenological consequence of introducing neutrino masses, and consequently lepton flavour mixing, is that the flavour of neutrinos *oscillates* during their propagation. That is, since flavour eigenstates are not propagation eigenstates, a neutrino produced with a given flavour could, after travelling, be detected as a neutrino of a different flavour.

Getting into more detail, a flavour eigenstate neutrino produced in a weak interaction process, $|\nu_\alpha\rangle$, will in general be a superposition of mass eigenstates

$$|\nu_\alpha\rangle = \sum_{i=1}^{n} U^{\text{lep}*}_{\alpha i} |\nu_i\rangle \,, \tag{1.10}$$

where the sum runs over light neutrino mass eigenstates. The origin of the complex conjugation is that $|\nu_\alpha\rangle \propto \bar{\nu}_\alpha |0\rangle = \sum_i U^{\text{lep}*}_{\alpha i} \bar{\nu}_i |0\rangle \propto \sum_i U^{\text{lep}*}_{\alpha i} |\nu_i\rangle$.

After travelling a distance L for a time t, the state of the neutrino will be

$$e^{-i\left(\hat{H}t - \hat{p}L\right)} |\nu_\alpha\rangle \,, \tag{1.11}$$

where $\hat{H}$ and $\hat{p}$ are the Hamiltonian and momentum operators, respectively. They are diagonal in the mass eigenstate basis, and for ultra-relativistic neutrinos

$$e^{-i\left(\hat{H}t-\hat{p}L\right)}\left|\nu_\alpha\right\rangle = \sum_{i=1}^{n} U_{\alpha i}^{\mathrm{lep}*} e^{-i\frac{m_i^2 L}{2E}}\left|\nu_i\right\rangle \,, \tag{1.12}$$

up to a constant phase. m_i is the mass of the i-th eigenstate and E is the average energy of the neutrino wave packet [25].

Therefore, the probability $P_{\alpha\beta}$ that the neutrino will be detected in a charged-current process associated to a flavour $|\nu_\beta\rangle$ is given by

$$\begin{aligned} P_{\alpha\beta} = 0 \left|\langle\nu_\beta|e^{-i\left(\hat{H}t-\hat{p}L\right)}|\nu_\alpha\rangle\right|^2 &= \left|\sum_{i=1}^{n} U_{\alpha i}^{\mathrm{lep}*} U_{\beta i}^{\mathrm{lep}} e^{-i\frac{m_i^2}{2E}}\right|^2 \\ &= \delta_{\alpha\beta} - 4\sum_{i<j}^{n} \mathrm{Re}\left[U_{\alpha i}^{\mathrm{lep}} U_{\beta i}^{\mathrm{lep}*} U_{\alpha j}^{\mathrm{lep}*} U_{\beta j}^{\mathrm{lep}}\right] \sin^2\frac{\Delta m_{ij}^2 L}{4E} \\ &\quad + 2\sum_{i<j}^{n} \mathrm{Im}\left[U_{\alpha i}^{\mathrm{lep}} U_{\beta i}^{\mathrm{lep}*} U_{\alpha j}^{\mathrm{lep}*} U_{\beta j}^{\mathrm{lep}}\right] \sin\frac{\Delta m_{ij}^2 L}{2E} \,, \end{aligned} \tag{1.13}$$

where $\Delta m_{ij}^2 \equiv m_i^2 - m_j^2$. The oscillation probability for antineutrinos is obtained exchanging $U^{\mathrm{lep}} \to U^{\mathrm{lep}*}$, thus modifying the sign of the last term. Thus, the oscillation probability can be different for neutrinos and antineutrinos, and CP violation in the leptonic sector can be detected studying this phenomenon.

Several aspects of Eq. (1.13) are to be noticed. In general, to have mass-induced flavour-oscillations neutrinos must have different masses ($\Delta m_{ij}^2 \neq 0$) and must mix ($U_{\alpha i}^{\mathrm{lep}} U_{\beta i}^{\mathrm{lep}} \neq \delta_{\alpha\beta}$). Besides, the particular functional form makes the Majorana phases in Eq. (1.8) cancel out when multiplying $U_{\alpha i}^{\mathrm{lep}} U_{\beta i}^{\mathrm{lep}*}$, so they are not observable. This is expected: the oscillation does not depend on the Dirac or Majorana nature of the neutrinos. Lastly, expression (1.13) has an oscillatory behaviour with characteristic oscillation lengths

$$L_{ij}^{\mathrm{osc}} = \frac{4\pi E}{\left|\Delta m_{ij}^2\right|} = (4\pi\hbar c)\frac{E}{\left|\Delta m_{ij}^2\right|} \simeq 2.48\frac{E|_{\mathrm{GeV}}}{\left|\Delta m_{ij}^2\right|_{\mathrm{eV}^2}}\,\mathrm{km}\,. \tag{1.14}$$

Since in real experiments neutrino beams are not monoenergetic but an incoherent superposition of different energy states and detectors have finite energy resolution, experiments do not measure $P_{\alpha\beta}$ but an average of it over some energy range. Thus, depending on the length L that neutrinos travel in an experiment, three different cases can be distinguished:

- $L \ll L_{ij}^{\mathrm{osc}}$: in this case, oscillations do not have enough time to develop, the sines in Eq. (1.13) are small and neither Δm_{ij}^2 nor the leptonic mixing matrix elements $U_{\alpha i}^{\mathrm{lep}}$ are measurable.
- $L \sim L_{ij}^{\mathrm{osc}}$: in this, case a well-designed experiment is sensitive to both Δm_{ij}^2 and the leptonic mixing matrix elements.
- $L \gg L_{ij}^{\mathrm{osc}}$: in this case, the oscillation phase goes through many cycles when averaging over the energy and $\sin^2\frac{\Delta m_{ij}^2 L}{4E}$ is averaged out to $\frac{1}{2}$. The experiment can be sensitive to the leptonic mixing matrix elements but not to Δm_{ij}^2.

This behaviour can also be understood graphically. Figure 1.1 represents the $\nu_e \to \nu_e$ (Fig. 1.1a) and $\nu_\mu \to \nu_\mu$ (Fig. 1.1b) oscillation probabilities as a function of the energy to distance ratio E/L for a three light neutrino paradigm with the oscillation parameters given in Ref [3]. In this scenario, there are three non-independent oscillation lengths, $\frac{E|_{\mathrm{GeV}}}{L_{21}^{\mathrm{osc}}\big|_{\mathrm{km}}} \simeq 3.02\cdot10^{-5}$, $\frac{E|_{\mathrm{GeV}}}{L_{23}^{\mathrm{osc}}\big|_{\mathrm{km}}} \simeq 9.88\cdot10^{-4}$, and $\frac{E|_{\mathrm{GeV}}}{L_{13}^{\mathrm{osc}}\big|_{\mathrm{km}}} = \frac{E|_{\mathrm{GeV}}}{L_{23}^{\mathrm{osc}}\big|_{\mathrm{km}}+L_{21}^{\mathrm{osc}}\big|_{\mathrm{km}}} \simeq 9.57\cdot10^{-4}$. Figure 1.1a shows the transition between the regions where L_{21}^{osc}, L_{23}^{osc}, or none contribute: L_{13}^{osc} is suppressed with respect

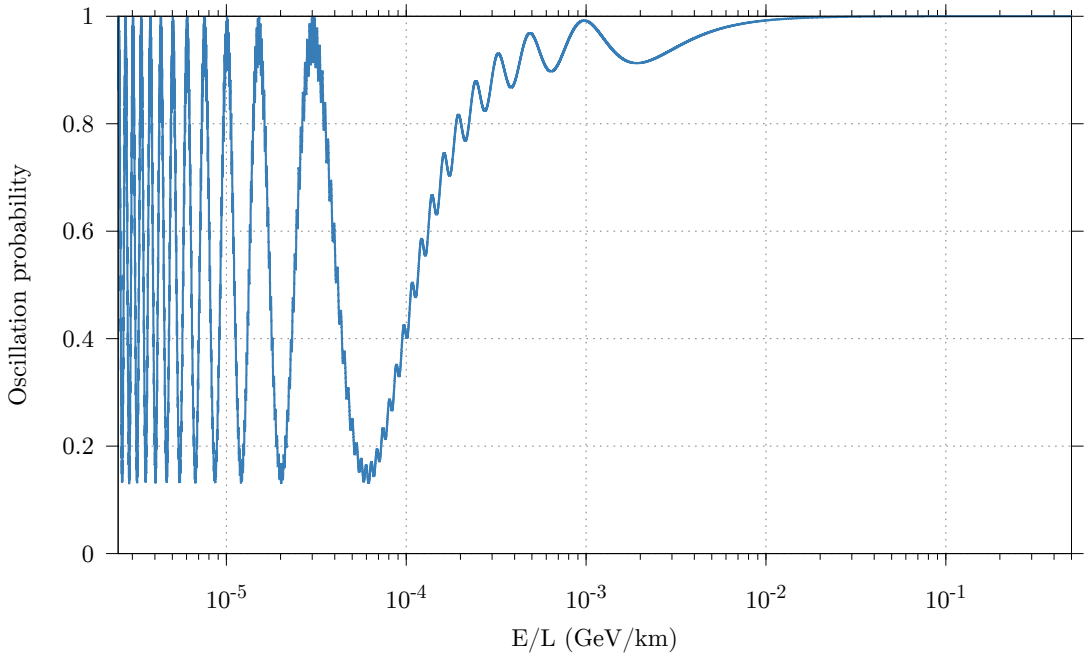

(a) $\nu_e \to \nu_e$ oscillation probability.

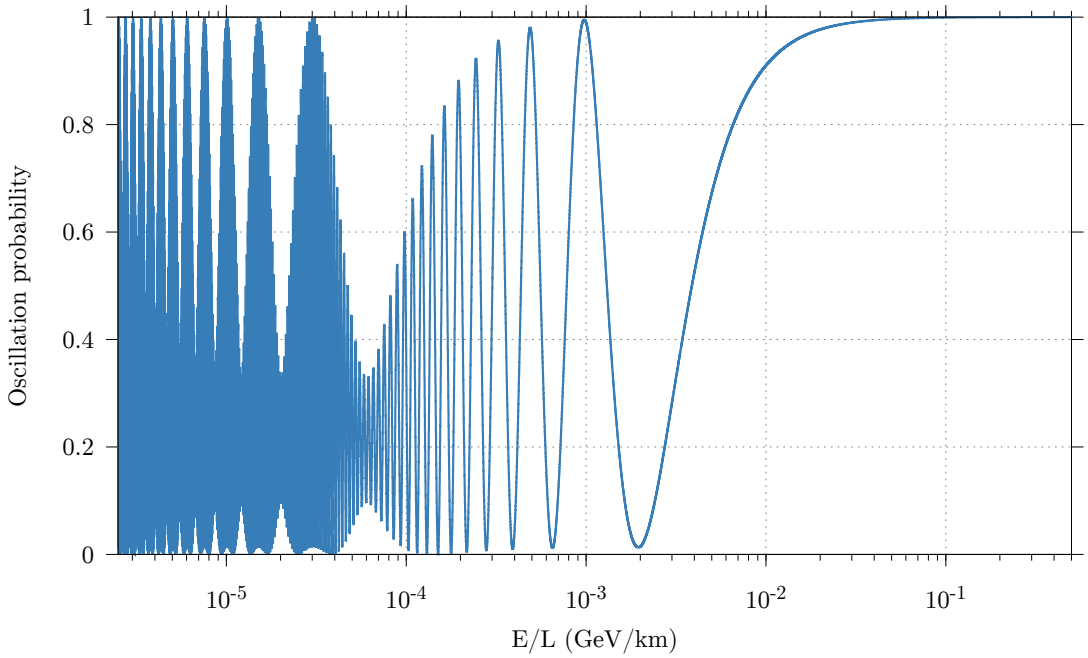

(b) $\nu_\mu \to \nu_\mu$ oscillation probability.

Figure 1.1: Some neutrino oscillation probabilities. The results have been obtained using Eq. (1.13) under the assumption of 3 light neutrinos and the values for the oscillation parameters in Ref. [3].

to $L_{23}^{\rm osc}$ because of their similar oscillation frequencies and the smallness of $U_{13}^{\rm lep} < U_{12}^{\rm lep}$. Nevertheless, since $U_{23}^{\rm lep} \sim U_{22}^{\rm lep}$, Fig. 1.1b shows the beats that typically appear when two oscillations of similar frequencies superpose.

Due to the three different oscillation regimes described above, some experimental results can be roughly understood in terms of an approximate two neutrino mixing. In that case, there is an angle dominantly controlling the observable oscillation amplitude and a mass difference dominantly controlling the observable frequency.

In detail, for 2 light neutrino generations $U^{\rm lep}$ is parametrised by a single angle θ and the oscillation formula is then quite simple:

$$P_{\alpha\beta} = \delta_{\alpha\beta} - (2\delta_{\alpha\beta} - 1)\sin^2 2\theta \sin^2 \frac{\Delta m^2 L}{4E}\,, \tag{1.15}$$

where Δm^2 is the squared mass difference between the considered mass eigenstates. In this case, the oscillation probability is symmetric under the exchange $\theta \leftrightarrow \frac{\pi}{2} - \theta$ and/or $\Delta m^2 \leftrightarrow -\Delta m^2$. Furthermore, no physical CP violating phase is left here. More-than-two neutrino mixing as well as matter effects (see below) break all these symmetries.

1.1.4 Matter effects

The oscillation probability calculation in Eq. (1.13) assumed that neutrinos travelled in vacuum. Even though their inelastic scattering cross section is very small, coherent forward elastic scattering on dense matter over long distances can significantly affect their properties. A detailed calculation shows that charged current interactions induce an effective Hamiltonian for ν_e in matter

$$H_{\rm eff} = \sqrt{2} G_F n_e \bar{\nu}_{eL} \gamma^0 \nu_{eL}\,, \tag{1.16}$$

where G_F is the Fermi constant and n_e the electron density at each point of the neutrino trajectory. This leads to an effective potential difference between electron neutrinos and other flavours

$$V_{\rm eff} = \pm\sqrt{2} G_F n_e\,, \tag{1.17}$$

where the + (-) sign refers to neutrinos (antineutrinos). Adding it to the free Hamiltonian, the oscillation probability for 3 light neutrinos travelling through matter of constant density (which is a good approximation for neutrinos studied in longbaseline accelerator experiments) is given by

$$P_{\alpha\beta} = |\mathcal{M}_{\beta\alpha}|^2\,, \tag{1.18}$$

with

$$\mathcal{M} = \exp\left\{-iL\left[\begin{pmatrix}\sqrt{2}G_F n_e & 0 & 0\\ 0 & 0 & 0\\ 0 & 0 & 0\end{pmatrix} + \frac{1}{2E} U^{\rm lep} \begin{pmatrix}0 & 0 & 0\\ 0 & \Delta m_{21}^2 & 0\\ 0 & 0 & \Delta m_{31}^2\end{pmatrix} U^{\rm lep\dagger}\right]\right\}\,, \tag{1.19}$$

where $U^{\rm lep}$ is the leptonic mixing matrix (1.8). In general there is no compact exact expression for this probability.

Nevertheless, there is an interesting effect: after global rephasings that do not affect the final result, the leptonic mixing matrix can be written as

$$U^{\rm lep} = \begin{pmatrix}1 & 0 & 0\\ 0 & c_{23}e^{-i\delta_{\rm CP}} & s_{23}\\ 0 & -s_{23}e^{-i\delta_{\rm CP}} & c_{23}\end{pmatrix}\begin{pmatrix}c_{13} & 0 & s_{13}\\ 0 & 1 & 0\\ -s_{13} & 0 & c_{13}\end{pmatrix}\begin{pmatrix}c_{12} & s_{12} & 0\\ -s_{12} & c_{12} & 0\\ 0 & 0 & 1\end{pmatrix} \equiv U_{23}U_{13}U_{12}\,, \tag{1.20}$$

with $U_{23}^\dagger \begin{pmatrix}\sqrt{2}G_F n_e & 0 & 0\\ 0 & 0 & 0\\ 0 & 0 & 0\end{pmatrix} U_{23} = \begin{pmatrix}\sqrt{2}G_F n_e & 0 & 0\\ 0 & 0 & 0\\ 0 & 0 & 0\end{pmatrix}$. Therefore,

$$\begin{aligned} U^{\rm lep\dagger}\mathcal{M}U^{\rm lep} \equiv& \tilde{\mathcal{M}}\\ =& \exp\left\{-iL\left[U_{12}^\dagger U_{13}^\dagger \begin{pmatrix}\sqrt{2}G_F n_e & 0 & 0\\ 0 & 0 & 0\\ 0 & 0 & 0\end{pmatrix} U_{13}U_{12} + \frac{1}{2E}\begin{pmatrix}0 & 0 & 0\\ 0 & \Delta m_{21}^2 & 0\\ 0 & 0 & \Delta m_{31}^2\end{pmatrix}\right]\right\}\,, \end{aligned} \tag{1.21}$$

which is independent of θ_{23} and $\delta_{\rm CP}$. That is, despite its complicated form, $\mathcal{M}$ can be written up to global rephasings as

$$\mathcal{M} = U_{23}^{\rm lep} \tilde{\mathcal{M}} U_{23}^{\rm lep\dagger} \,, \tag{1.22}$$

with $\tilde{\mathcal{M}}$ independent of θ_{23} and $\delta_{\rm CP}$.

As a consequence, a two neutrino scenario gets significantly modified by matter effects (take for example $\nu_\mu \leftrightarrow \nu_e$ oscillations by setting $\theta_{13} = \theta_{23} = 0$). There, the presence of the matter potential allows to distinguish the sign of Δm^2_{12} (or, equivalently, whether $\theta_{12} < 45^\circ$ or not). I also induces a different oscillation probability between neutrinos and antineutrinos, this is, matter breaks CP because it contains only electrons and not positrons.

Matter effects play a fundamental role in the flavour evolution of solar neutrinos. For solar neutrinos the matter density cannot be considered constant along the neutrino propagation so the derivation of the relevant oscillation probability is more involved. In particular, it presents the so-called MSW effect [26, 27], which explains the observed deficit of solar neutrinos.

1.1.5 Leptonic CP violation as a consequence of neutrino masses

Besides flavour-oscillations, another important consequence of neutrino masses and mixing is the possibility of having CP violation in the leptonic sector. As in the quark sector, flavour mixing between 3 particle generations opens the door to breaking this symmetry. In particular, a non zero value for any of the phases in the parametrisation (1.8) will introduce a phase in the Lagrangian that violates CP. For the rest of this work, the Majorana phases will be ignored: they depend on the Dirac or Majorana nature of neutrino mass eigenstates but, as discussed above, they are irrelevant for neutrino oscillations.

The fact that a non zero value of $\delta_{\rm CP}$ can lead to CP violation is directly present in the oscillation formula (1.13): due to the chiral structure of the SM, antineutrinos (right-handed) are the CP conjugates of neutrinos (left-handed); any difference in $P_{\alpha\beta}$ between neutrinos and antineutrinos is a sign of CP violation. Since Eq. (1.13) accounts for antineutrino oscillations just by substituting $U^{\rm lep} \to U^{\rm lep*}$, only the terms in the second sum

$$\mathrm{Im}\left[U_{\alpha i}^{\rm lep*} U_{\beta i}^{\rm lep} U_{\alpha j}^{\rm lep*} U_{\beta j}^{\rm lep}\right] \,, \, i < j \,, \, \alpha \neq \beta \tag{1.23}$$

violate CP. It is immediate to see that if $\delta_{\rm CP} \neq 0$ these elements are different from zero. Furthermore, for three light neutrinos the matrix element products (1.23) can be shown to be all equal, up to signs, to

$$c_{12} c_{23} c_{13}^2 s_{12} s_{23} s_{13} \sin\delta_{\rm CP} \,. \tag{1.24}$$

This quantity is called the Jarlskog invariant J. It is invariant under phase redefinitions; thus, it provides a parametrisation-independent way of quantifying CP violation [28].

1.2 Experimental study of neutrino oscillations

Even if neutrino masses are tiny, their low interaction cross section allows to work with neutrinos whose path extends over long distances and are thus sensitive to oscillation effects. Furthermore, thanks to the advances in efficient detection techniques, the particles that neutrinos scatter with can be efficiently observed. The experimental study of neutrino physics is, then, a matter of building large enough detectors. This new window to flavour phenomena grants empirical access to beyond SM physics [29] and therefore its study is of great interest.

The first step, however, is to check that leptonic flavours do oscillate in neutrino propagation as a consequence of neutrino masses. Historically, neutrino masses and mixing were proposed to successfully explain a deficit in the Solar neutrino flux [19], but any other mechanism introducing a distinction between interaction and propagation eigenstates could explain the same phenomenon. Some alternatives, which generally introduce a dependence of the flavour-oscillation probability on the energy different from $\sim \sin\frac{L}{E}$, include neutrino decay, quantum decoherence, or Lorentz invariance violation. Nevertheless, the precise analysis of neutrino spectra and the direct detection of neutrinos with a flavour different from the one with which they were generated conclusively proved that the observed phenomena were mass-induced flavour-oscillations.

1.2.1 Constraining the mixing parameters

Once mass-induced neutrino oscillations are experimentally established, the next step is to characterise their properties. Apart from some experimental tensions [30–33] that do not have enough significance [3, 17], all the existing oscillation data can be explained by a three light neutrino paradigm parametrised by the mixing matrix (1.8). The convention regarding the numbering of mass eigenstates, diagrammatically shown in Fig. 1.2, makes use of the experimental fact (see description of the data below) that two of them have masses close to each other ($\Delta m^2 \sim 10^{-5}\,\mathrm{eV}^2$) whereas the third one is further away ($\Delta m^2 \sim 10^{-3}\,\mathrm{eV}^2$). Based on this, one can always chose a convention in which the close eigenstates are denoted as ν_1 and ν_2 with $m_1 < m_2$ keeping the ranges of angles and phases as $\theta_{12}, \theta_{13}, \theta_{23} \in [0, 90°]$, and $\delta_{\mathrm{CP}} \in [0, 2\pi]$. The other eigenstate is denoted as ν_3. It is currently unknown whether $m_3 > m_1$ (denoted as Normal Ordering, NO) or $m_3 < m_1$ (denoted as Inverted Ordering, IO).

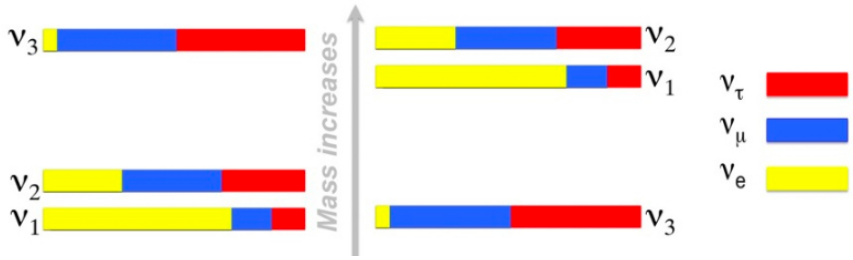

Figure 1.2: Convention for the numbering of mass eigenstates and possible orderings (NO in left, IO in right). The colours indicate the amount of mixing between mass and flavour eigenstates. Source: Ref. [34].

Due to the different oscillation regimes described in Sec. 1.1.3 and explicitly seen in Fig. 1.1, there are qualitatively different experiments that look for different aspects of the neutrino mixing matrix. In general, they can be classified in four categories.

Solar neutrinos Neutrinos from the Sun played an important role in the historical development of neutrino physics. In the nuclear reactions that take place in our star, electron neutrinos of energies $\sim$ MeV are abundantly produced. Even if the oscillation lengths are much smaller than the distance between the Sun and the Earth, matter effects significantly affect the evolution of ν_1 and ν_2 [26, 27], and therefore experiments that detect neutrinos from the Sun can measure θ_{12}, θ_{13} and Δm^2_{21}. For the Sun, however, the approximation of constant matter presented in Sec. 1.1.4 does not hold and the corresponding oscillation probability is more complex. Examples of Solar experiments are SuperKamiokande [35], a 50 000 ton water tank Cherenkov detector, Borexino [36], a 300 ton liquid scintillator calorimeter, or SNO [37], a 1000 ton heavy water Cherenkov detector. Their results lead to the determination of one of the mass splittings $\Delta m^2_{21} \sim \mathcal{O}(10^{-5}\mathrm{eV}^2)$ and one mixing angle $\theta_{12} \sim 30°$.

Atmospheric neutrinos Muon and electron neutrinos and antineutrinos are abundantly produced in particle cascades created when cosmic rays hit the atmosphere. They have been detected with energies from hundreds of MeV up to hundreds of GeV, and they travel for distances ranging from 10 km to 10^4 km, depending on the incident angle [16]. Since $L^{\mathrm{osc}}_{12}|_{\mathrm{km}} \sim 10^5\, E|_{\mathrm{GeV}}$, experiments detecting atmospheric neutrinos are almost insensitive to the mass splitting determined by Solar experiments. Nevertheless, $L^{\mathrm{osc}}_{23}|_{\mathrm{km}} \sim 10^3\, E|_{\mathrm{GeV}}$, so atmospheric experiments are mostly sensitive to Δm^2_{32} (or, equivalently, $\Delta m^2_{31} = \Delta m^2_{32} + \Delta m^2_{21}$) and θ_{23}. There is also some marginal dependence on δ_{CP} and θ_{13}. Examples of atmospheric neutrino experiments are SuperKamiokande [15] or DeepCore [16], an array of photomultipliers buried in the South Pole ice that detect Cherenkov light. Their results lead to the determination of $|\Delta m^2_{31}| \sim \mathcal{O}(10^{-3}\mathrm{eV}^2)$ and $\theta_{23} \sim 45°$.

Reactor neutrinos Solar and atmospheric neutrino experiments alone could only put upper bounds in the mixing angle θ_{13}; to directly measure it a new set of experiments using electron

antineutrinos from nuclear reactors was proposed. Reactor experiments usually employ two detectors, one close to the reactor and the other one at a distance $\sim L_{13}$ (i.e., experiments are sensitive to oscillations driven by Δm^2_{31}), so that systematic uncertainties cancel among them. These neutrinos have energies of few MeV, so $L^{\text{osc}}_{13} \sim 1$ km. Examples of reactor neutrino experiments are Daya Bay [14], Double Chooz [38], and RENO [39], whose detectors are essentially vessels filled with liquid scintillator. Their results have allowed to determine $\theta_{13} \sim 9^\circ$. Another experiment, KamLAND, is worth mentioning: its far detector is at a longer distance ~ 100 km, which allows it to verify and complement Solar data by independently measuring θ_{12}, θ_{13} and Δm^2_{21}.

Accelerator neutrino experiments All the experiments mentioned up to now do not have control over the neutrino source, which difficults fine-tuned precision measurements and adds systematic uncertainties. Because of that, some neutrino experiments, called accelerator neutrino experiments, employ an *ex profeso* created beam of neutrinos. The baselines of these experiments are of several hundred kilometres, the reason for which they are usually referred to as long baseline (LBL) experiments. A common method to create a neutrino beam makes use of the following reaction chain initiated by hitting a dense target with a beam of high energetic protons:

$$\begin{aligned} p + \textit{target} \longrightarrow \pi^\pm + X & \\ \pi^+ \quad \longrightarrow \mu^+ \nu_\mu & \\ \mu^+ \quad \longrightarrow e^+ \nu_e \bar{\nu}_\mu & \\ \pi^- \quad \longrightarrow \mu^- \bar{\nu}_\mu & \\ \mu^- \quad \longrightarrow e^- \bar{\nu}_e \nu_\mu & \end{aligned} \qquad . \tag{1.25}$$

This reaction creates a beam of ν_μ, ν_e, $\bar{\nu}_\mu$ and $\bar{\nu}_e$, whose abundance can be controlled by separating the positive and negative pion beams with a magnetic field and stopping the muons with enough solid material. Since neutrinos are produced in a two-body decay, their energy is fixed and their spectrum can be controlled by focusing the pion beam. Furthermore, the possibility of easily switching between a neutrino-dominated beam and an antineutrino-dominated beam allows to easily test CP violation. The same process can also be mediated by kaons instead of pions, but the branching ratio of purely leptonic decays from kaons is $\sim 64\%$ compared with $\sim 99.99\%$ from pions [18].

This process creates neutrinos with energies $\sim$ GeV; thus, oscillation lengths $L^{\text{osc}}_{21} \sim 10^5$ km and $L^{\text{osc}}_{23} \sim 10^3$ km. By placing a detector far away from the source, thus making the neutrino beam travel underground, Δm^2_{32} and θ_{23} can be measured. What is more, observing the appearance of electron (anti)neutrinos in a muon (anti)neutrino beam opens a clear experimental window to the measurement of θ_{13}, δ_{CP} and the mass ordering. Getting into more detail, the $\nu_\mu \to \nu_e$ oscillation probability in constant matter density is approximately given by [40]

$$\begin{aligned} P\left(\nu_\mu \to \nu_e\right) = \sin^2\theta_{23} \sin^2 2\theta_{13} \frac{\sin^2 \Delta(1-A)}{(1-A)^2} & \\ + \frac{\Delta m^2_{21}}{\Delta m^2_{31}} \cos\theta_{13} \sin 2\theta_{13} \sin 2\theta_{12} \sin 2\theta_{23} \cos\left(\Delta \pm \delta_{\text{CP}}\right) \frac{\sin \Delta A}{A} \frac{\sin \Delta(1-A)}{(1-A)} & \\ + \left(\frac{\Delta m^2_{21}}{\Delta m^2_{31}}\right)^2 \cos^2\theta_{23} \sin^2 2\theta_{12} \frac{\sin^2 \Delta A}{A^2} + \mathcal{O}\left(\frac{\Delta m^2_{21}}{\Delta m^2_{31}}\right)^3 , & \end{aligned} \tag{1.26}$$

where $\Delta \equiv \Delta m^2_{31} \frac{L}{4E}$, $A = \pm 2\sqrt{2} G_F n_e \frac{E}{\Delta m^2_{31}}$, the plus (minus) signs apply to neutrinos (antineutrinos), and n_e is the electron number density in the Earth matter travelled by neutrinos. The latter variable is assumed to be constant, which is a good approximation for the Earth crust crossed in these experiments.

As it is seen, with a precise measurement of other parameters, this expression is sensitive to θ_{13}, the sign of Δm^2_{31} (the mass ordering) and δ_{CP}.

A large experimental effort is being put towards this kind of experiments. Some examples include T2K, a beam that travels for 295 km before arriving to the Super Kamiokande detector, MINOS, a beam that travels for 700 km from Fermilab to the Soudan Mine in Minnesota, and NOνA, a beam that travels for 800 km from Fermilab to Ash River in Minnesota. The latter has been the main subject of study in this work.

1.2.2 Current status

After combining more than 40 years of neutrino data, a global fit published before the work carried out here [3] gave the following results for neutrino oscillation parameters:

- The "Solar" parameters θ_{12} and Δm^2_{21} were known with more than 15% precision[2] at 3σ.
- The "reactor" parameter θ_{13} was known with more than 15% precision at 3σ.
- The "atmospheric" parameters θ_{23} and Δm^2_{32} were known less accurately: the precision at 3σ of θ_{23} was $\sim 33\%$ and its octant (whether $\theta_{23} > 45°$, first octant, or $\theta_{23} < 45°$, second octant) was unknown. The precision for $|\Delta m^2_{32}|$ was $\sim 12\%$ but the confidence on its sign did not even reach 1σ.
- No value of $\delta_{\rm CP}$ was discarded with a 3σ confidence.

The ignorance on the θ_{23} octant, the sign of Δm^2_{32}, and the value of $\delta_{\rm CP}$ can be traced back to the insensitivity to these properties in the vacuum two-neutrino mixing approximation. In order to disentangle them, three neutrino mixing and/or matter effects are needed, both suppressed by the small value of θ_{13} and $\Delta m^2_{21} \ll |\Delta m^2_{32}|$.

Table 1.1 shows the specific best-fit values of the oscillation parameters; Figures 1.3 and 1.4 show correlations between some of them.

	Normal Ordering ($\Delta\chi^2 = 0.97$)		Inverted Ordering (best fit)		Any Ordering
	bfp $\pm 1\sigma$	3σ range	bfp $\pm 1\sigma$	3σ range	3σ range
$\sin^2\theta_{12}$	$0.304^{+0.013}_{-0.012}$	$0.270 \to 0.344$	$0.304^{+0.013}_{-0.012}$	$0.270 \to 0.344$	$0.270 \to 0.344$
$\theta_{12}/^\circ$	$33.48^{+0.78}_{-0.75}$	$31.29 \to 35.91$	$33.48^{+0.78}_{-0.75}$	$31.29 \to 35.91$	$31.29 \to 35.91$
$\sin^2\theta_{23}$	$0.452^{+0.052}_{-0.028}$	$0.382 \to 0.643$	$0.579^{+0.025}_{-0.037}$	$0.389 \to 0.644$	$0.385 \to 0.644$
$\theta_{23}/^\circ$	$42.3^{+3.0}_{-1.6}$	$38.2 \to 53.3$	$49.5^{+1.5}_{-2.2}$	$38.6 \to 53.3$	$38.3 \to 53.3$
$\sin^2\theta_{13}$	$0.0218^{+0.0010}_{-0.0010}$	$0.0186 \to 0.0250$	$0.0219^{+0.0011}_{-0.0010}$	$0.0188 \to 0.0251$	$0.0188 \to 0.0251$
$\theta_{13}/^\circ$	$8.50^{+0.20}_{-0.21}$	$7.85 \to 9.10$	$8.51^{+0.20}_{-0.21}$	$7.87 \to 9.11$	$7.87 \to 9.11$
$\delta_{\rm CP}/^\circ$	306^{+39}_{-70}	$0 \to 360$	254^{+63}_{-62}	$0 \to 360$	$0 \to 360$
$\frac{\Delta m^2_{21}}{10^{-5}\ \text{eV}^2}$	$7.50^{+0.19}_{-0.17}$	$7.02 \to 8.09$	$7.50^{+0.19}_{-0.17}$	$7.02 \to 8.09$	$7.02 \to 8.09$
$\frac{\Delta m^2_{3\ell}}{10^{-3}\ \text{eV}^2}$	$+2.457^{+0.047}_{-0.047}$	$+2.317 \to +2.607$	$-2.449^{+0.048}_{-0.047}$	$-2.590 \to -2.307$	$\begin{bmatrix}+2.325 \to +2.599\\ -2.590 \to -2.307\end{bmatrix}$

Table 1.1: Results of global fit to neutrino oscillation parameters as of September 2014. "bfp" stands for best fit point. $\Delta m^2_{3\ell}$ refers to Δm^2_{31} for NO and Δm^2_{32} for IO. Table extracted from Ref [3].

As can be seen in Figs. 1.3 and 1.4, most correlations appear between the less-known parameters Δm^2_{32}, θ_{23} and $\delta_{\rm CP}$, which can be studied and constrained with long baseline neutrino experiments. In particular, as Eq. (1.26) shows, they offer unique sensitivity to the mass ordering, the θ_{23} octant, and $\delta_{\rm CP}$. Because of that, there is a firm experimental programme aimed at these experiments that, combined, could shed light on these parameters [6, 41, 42].

[2]The precision for an interval $[x_{\rm low}, x_{\rm up}]$ is defined as $\frac{x_{\rm up}-x_{\rm low}}{(x_{\rm up}-x_{\rm low})/2}$.

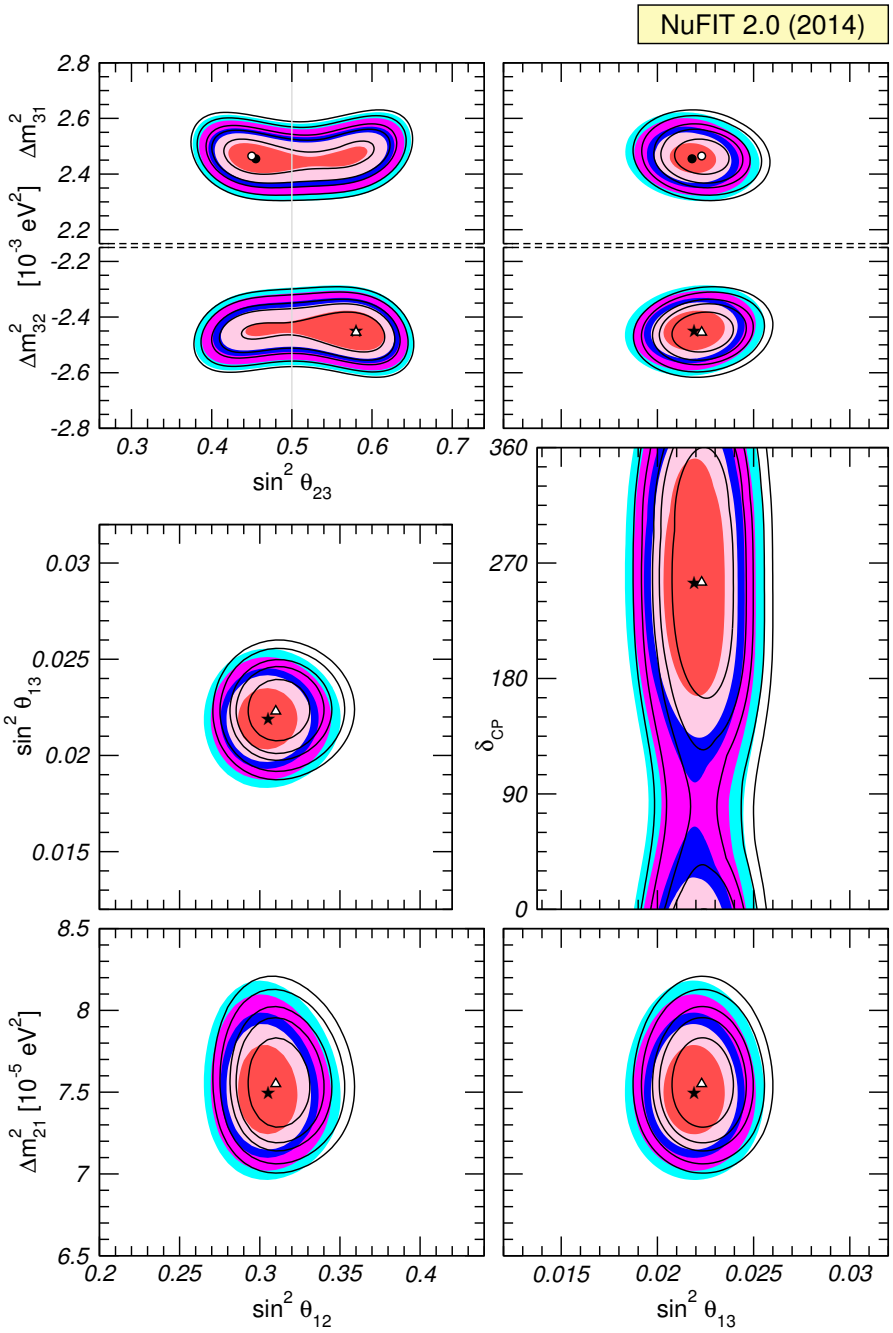

Figure 1.3: Correlations between several parameters. Each panel shows the two-dimensional projection of the allowed six-dimensional region after marginalisation with respect to the undisplayed parameters. The different contours correspond to the two-dimensional allowed regions at 1σ, 90%, 2σ, 99%, 3σ confidence level. For the same panel, different best fits and contours use different data from reactor experiments. Source: Ref. [3].

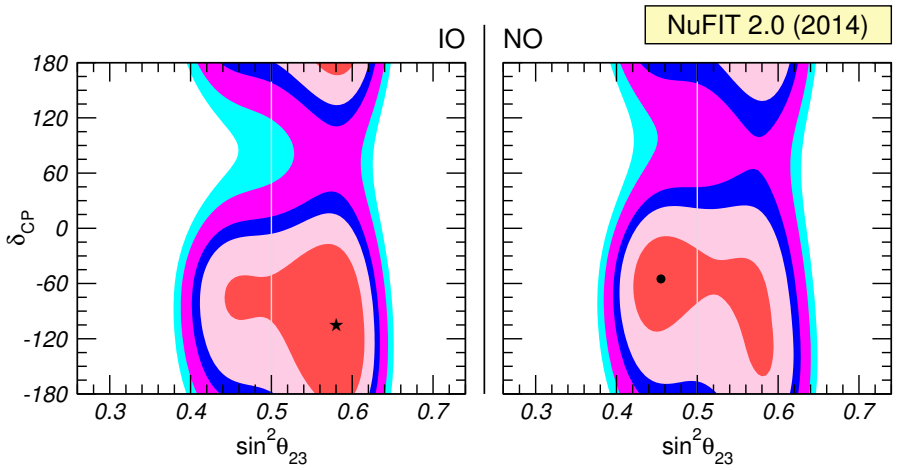

Figure 1.4: Correlation between δ_{CP} and θ_{23} for different mass orderings. See caption in Fig. 1.3 for the explanation about the points and contours. Source: Ref. [3].

In particular, in January 2016 the first results from the NOνA experiment came out [11, 12]. The subject of this work has been to independently analyse those results and combine them with the ones discussed in this section in order to produce an up-to-date global fit.

Chapter 2

The NOνA experiment

This work has focused on the study of data from the NOνA experiment. The experiment, a firm proposal of which was made in the year 2005 [43], makes use of the NuMI neutrino beam generator to send a muon neutrino beam from Fermilab, near Chicago, to Ash River, in Minnesota at about 800 Km of distance. It is particularly designed to efficiently detect electron neutrinos, and the beam spectrum is sharply peaked at 2 GeV, around the first $\nu_\mu \to \nu_e$ oscillation maximum.

2.1 Experimental design

The NOνA experiment has several parts whose understanding is fundamental to get a global view of it[1].

2.1.1 The NuMI beam generator

The first stage of the experiment is the NuMI neutrino beam generator, in Fermilab. It consists on a circular accelerator that accelerates protons to 120 GeV and makes them collide with a graphite target. As a result, pions and kaons of energies ~ 10 GeV are produced, which through the process (1.25) create a neutrino beam. Focusing the parent mesons allows to narrow the neutrino energy spectrum, whereas a magnetic horn selects the sign of their charge and thus whether the beam is mainly composed of neutrinos or antineutrinos.

Afterwards, there is a pipe of about 700 m (the decay length of pions with energy ~ 10 GeV), where pions and kaons decay. After a thick concrete wall that absorbs all remaining hadrons, a neutrino beam is in principle the only remnant.

There is an interesting subtlety regarding the orientation of the beam. Both pions and kaons, being spinless particles and their muonic decays two-body decays, emit in their rest frame neutrinos isotropically and with a fixed energy. Considering Lorentz boosts, however, the picture changes and isotropy is lost. In particular, in the laboratory frame the neutrino energy E_ν and flux ϕ_ν as a function of the angle θ with respect to the meson beam are given by

$$E_\nu(\theta) = \left(1 - \frac{m_\mu^2}{m_h^2}\right) \frac{E_h}{1 + \theta^2\gamma^2}\,, \tag{2.1}$$

$$\phi_\nu(\theta) = \left(\frac{2\gamma}{1 + \theta^2\gamma^2}\right)^2 \frac{1}{4\pi L^2}\,. \tag{2.2}$$

m_μ is the muon mass, m_h and E_h are the mass and energy of the decaying meson, γ is its Lorentz factor, and L is the distance at which the flux is measured. The values of E_ν and ϕ_ν as a function of the parent meson energy for neutrinos produced in pion decays are shown in Fig. 2.1. A narrow energy spectrum allows for a better measurement of neutrino oscillations, and it also helps in reducing backgrounds of different energy. Since an angle $\theta = 14$ mrad provides a fairly narrow energy spectrum while keeping an acceptable flux, NOνA detectors are displaced

[1] Unless otherwise specified, the information in this section has been extracted from Ref. [44].

14 mrad with respect to the NuMI beam direction. Fig. 2.2 compares the expected unoscillated neutrino spectrum for $\theta = 0$ and $\theta = 14$ mrad.

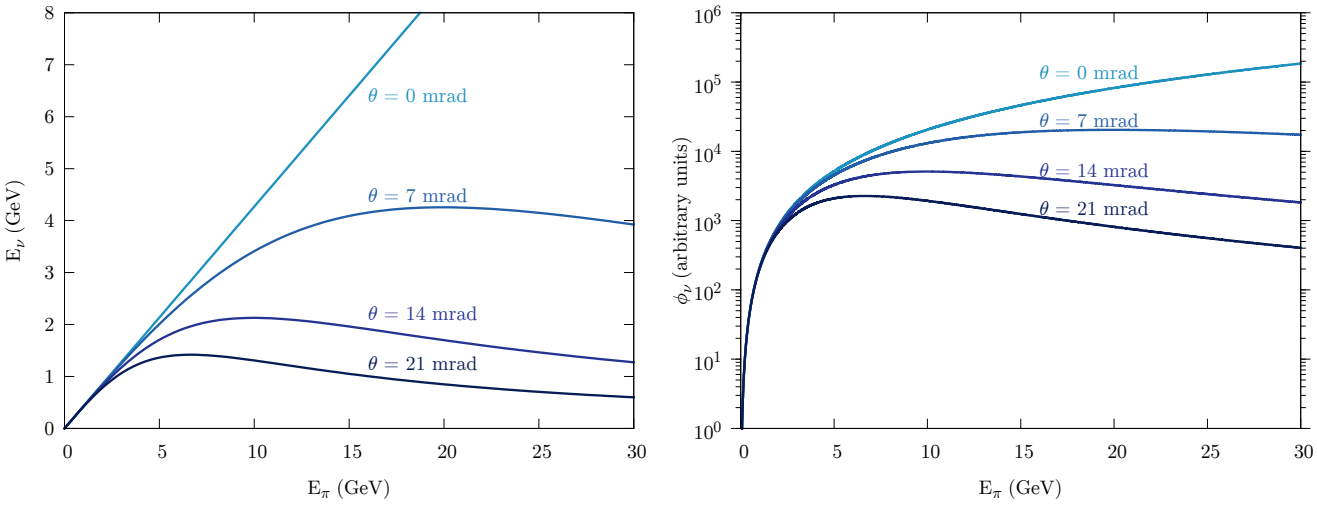

Figure 2.1: Neutrino energy (left) and flux (right) for different pion energies E_π.

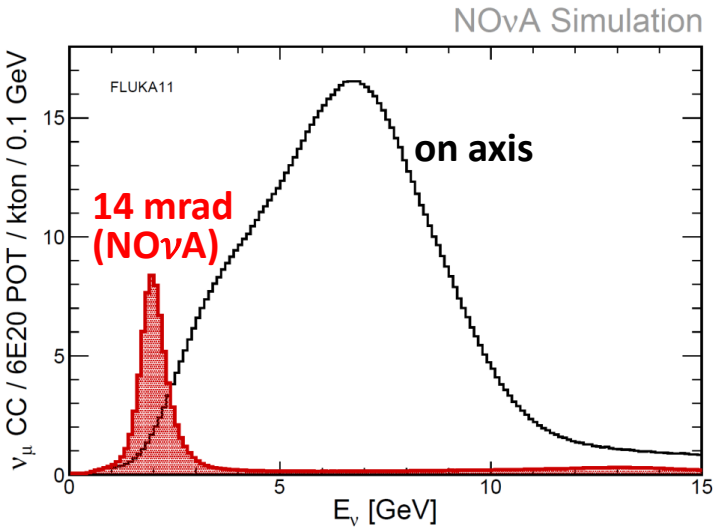

Figure 2.2: Expected spectrum of charged current events either for an on-axis detector (black) and for a 14 mrad off-axis detector (red). Source: Ref [45].

2.1.2 Near and far detectors

In order to reduce systematic uncertainties related both to the marginal presence of different neutrino flavours in the beam and to experimental uncertainties, NOνA has an underground detector located at Fermilab, close to the NuMI source.

This near detector is a segmented calorimeter made of cells filled with liquid scintillator. Signal events are detected through charged current interactions, which produce a lepton and a hadronic shower: adding up the energies of both particles the incident neutrino energy can be reliably reconstructed.

Finally, to detect neutrino oscillations NOνA has another detector designed exactly as the near detector but with a larger size and located 810 km away from it. Even though it is on

the surface, it is shielded from cosmic rays by a concrete and barite layer that is effectively 14 radiation lengths thick.

2.1.3 Signal selection and backgrounds

The NOνA experiment is characterised by a good measurement of the energy and flavour of incident neutrinos. As mentioned, for charged current interactions the neutrino energy is obtained by adding up the energies of all resulting particles. What is more, since muons are minimum-ionising particles whereas electrons produce a shower as they pass through matter, the topological properties of the leptonic part of the event allows to identify the neutrino flavour. For the particular case of ν_e identification, NOνA used two different algorithms: an artificial neural network based on energy deposition and topological properties of the event (LID, for Likelihood based particle ID) [46], and a boosted decision tree comparing the energy deposition in each detector cell with a vast library of simulated events (LEM, for Library Event Matching) [47].

Concerning the signal purity, the experiment is designed to efficiently reduce backgrounds from cosmic rays and neutral current interactions — the latter are considered background because from them neither the flavour nor the incident neutrino energy can be reconstructed. In more detail, cosmic backgrounds are diminished with the shielding of the detectors and the calorimeter segmentation, which allows to estimate the incident neutrino direction. Neutral current interactions, on the other hand, only deposit part of the neutrino energy in the calorimeter: the narrowness of the incident spectrum allows to severely reduce this background. Besides, there are backgrounds from missidentification and other neutrino flavours present in the beam that can be quantified with the help of the near detector.

All in all, from a quantitative point of view, the NOνA energy resolution[2] is 9% for electron neutrinos [46] and 7% for muon neutrinos [11]. Moreover, the far detector still has several systematic uncertainties once the near detector is included in the overall analysis. Effectively, they can be summarised in a normalisation uncertainty and an energy scale uncertainty, recorded in Table 2.1. The former is associated to uncertainties in the incident flux and neutrino cross sections as well as possible effects of the event selection procedure, whereas the latter is associated to absolute energy scale calibration errors.

	Systematic uncertainty (%)		
	ν_e events		ν_μ events
	LEM selection procedure	LID selection procedure	
Signal normalisation	15	17.6	1.4
Background normalisation	13.4	10.8	1.4
Energy scale	5	5	15

Table 2.1: Systematic uncertainties in the NOνA experiment. Since they are an effect of many underlying processes, the central limit theorem can be invoked to assume a Gaussian distribution for the uncertainties, so their standard deviations are quoted. Source: Refs. [11, 12, 46, 48].

It is worth mentioning the large energy scale uncertainty for ν_μ events: it stems from a large difference between predictions and near detector data for the hadronic energy deposited in neutrino interactions. The NOνA collaboration corrected it at a low level in their simulations, by explicitly modifying the hadronic energy to match near detector data and introducing a 100% systematic uncertainty in that modification [11].

2.2 Replication and analysis of NOνA results

The first official NOνA results came out in early 2016 [11,12]. An important original part of this work has been to reproduce them.

[2] The energy resolution is defined as the standard deviation of a Gaussian fit to the distribution of $\frac{E_{\text{true}}-E_{\text{reco}}}{E_{\text{true}}}$, where E_{reco} and E_{true} are, respectively, the reconstructed and true neutrino energies in a simulation of the whole experiment.

2.2.1 Statistical data analysis

Since neutrinos interact rather rarely, the NOνA results are dominated by large statistical uncertainties. Because of that, it is important to get familiarised with the statistical tools commonly used in neutrino physics.

Usually, analyses use a log-likelihood test to quantify the agreement between data and different hypotheses, i.e., different values for the neutrino oscillation parameters. In particular, for an experiment with data data_{exp} and for a set of oscillation parameters Θ, the log-likelihood for that experiment χ^2_{exp} is given by

$$\chi^2_{\text{exp}}(\Theta) = -\ln \mathcal{P}(\text{data}_{\text{exp}}|\Theta)\,, \tag{2.3}$$

where $\mathcal{P}(\text{data}_{\text{exp}}|\Theta)$ is the probability of obtaining the data points data_{exp} assuming the oscillation parameters to be Θ. The probabilistic nature stems both from systematic uncertainties in the experiment and from neutrino oscillations being described by quantum mechanics. The test statistic (2.3) is particularly useful because, for independent experiments, $\chi^2 = \sum_{\text{exp}} \chi^2_{\text{exp}}$.

The best fit parameters are chosen to be the ones that minimise $\chi^2(\Theta)$, whereas confidence intervals are obtained by evaluating

$$\Delta\chi^2(\Theta) = \chi^2(\Theta) - \min_{\Theta} \chi^2(\Theta)\,. \tag{2.4}$$

According to Wilk's theorem [49], in the large sample limit (what is usually known as the *Gaussian limit*) the test statistic (2.4) is distributed following a χ^2 distribution whose number of degrees of freedom is the number of parameters in Θ. Therefore, in the Gaussian limit, a $\Delta\chi^2$ confidence interval $[0, \Delta\chi^2_\lambda]$ with confidence level (CL) λ fulfils

$$\int_0^{\Delta\chi^2_\lambda} \chi^2_{\dim(\Theta)}(x)\,\mathrm{d}x = \lambda\,, \tag{2.5}$$

where $\chi^2_{\dim(\Theta)}(x)$ is a χ^2 distribution whose number of degrees of freedom is the number of parameters in Θ. Since $\chi^2 = \chi^2(\Theta)$, confidence intervals on χ^2 can be translated into confidence regions on Θ in a straightforward manner.

Table 2.2 shows numerically obtained values of $\Delta\chi^2_\lambda$ for difference confidence levels and different degrees of freedom.

CL (%)	$\Delta\chi^2_\lambda$	
	1 d.o.f.	2 d.o.f.
68.27	1.00	2.30
90.00	2.71	4.61
95.00	3.84	5.99
95.45	4.00	6.18
99.00	6.63	9.21
99.73	9.00	11.83

Table 2.2: Value of $\Delta\chi^2_\lambda$ corresponding to a given confidence level (CL) for different degrees of freedom (d.o.f.) of the underlying χ^2 distribution.

Nuisance parameters

Usually, the model to which the data is fitted contains additional parameters, referred to as nuisance parameters, different from the ones that are to be extracted from data. Examples include previously well-measured neutrino oscillation parameters or variables parametrising systematic uncertainties. In order to include their effect, the test statistics (2.3) and (2.4) are modified to

$$\chi^2_{\text{exp}}(\Theta) = \min_{\xi} \left[-\ln \mathcal{P}(\text{data}_{\text{exp}}|\Theta,\xi)\right] \equiv \min_{\xi} \chi^2\left(\Theta,\xi\right)\,, \tag{2.6}$$

and

$$\Delta\chi^2(\Theta) = \min_{\xi} \chi^2(\Theta,\xi) - \min_{\Theta,\xi} \chi^2(\Theta,\xi)\,, \tag{2.7}$$

respectively, where ξ are the nuisance parameters. This is equivalent to choosing as a value for ξ the one that, for each Θ, maximises the probability of having obtained data_{exp}. This way, possible correlations between ξ and Θ are taken into account.

General analysis strategy

It is relatively easy to compute $\chi^2\left(\Theta,\xi\right)$ for binned data such as the one obtained by NOνA. In general, if the average number of events in a bin i is calculated to be μ_i, the observed number of events n_i will be Poisson-distributed. If, additionally, there are several Gaussian-distributed nuisance parameters ξ_j around a mean ξ_j^0 and with a standard deviation σ_j, then

$$\mathcal{P}\left(\text{data}|\Theta,\xi\right) = \prod_{i,j} \frac{\mu_i^{n_i} e^{-\mu_i}}{n_i!} \frac{1}{\sigma_j\sqrt{2\pi}} e^{-\frac{\left(\xi_j-\xi_j^0\right)^2}{2\sigma_j^2}}\,. \tag{2.8}$$

The observed number of events per bin n_i as well as the nuisance parameters ξ_j have been assumed to be independent.

Dropping off terms that do not depend on (Θ,ξ) and are therefore irrelevant both for minimising χ^2 and for calculating $\Delta\chi^2$,

$$\chi^2\left(\Theta,\xi\right) = 2\sum_i \left(\mu_i - n_i + n_i \ln\frac{n_i}{\mu_i}\right) + \sum_j \frac{\left(\xi_j-\xi_j^0\right)^2}{\sigma_j^2}\,, \tag{2.9}$$

where the logarithmic term is taken to be 0 if $n_i = 0$. In general, $\mu_i = \mu_i\left(\Theta,\xi\right)$. Particularising for the NOνA analyses, *a priori* there are three nuisance parameters associated to systematic uncertainties: a signal normalisation factor $\xi_1 \equiv \eta_s$, a background normalisation factor $\xi_2 \equiv \eta_b$, and an absolute energy scale uncertainty $\xi_3 \equiv \rho$, all of them centred around 1. In that case, the prediction μ_i for a given energy bin $[E_i, E_{i+1}]$ is given by

$$\begin{aligned}\mu_i =& \eta_s \int_{\rho E_i}^{\rho E_{i+1}} \mathrm{d}E_{\text{reco}} \int_0^\infty \mathrm{d}E_{\text{true}} f_{\text{res}}\left(E_{\text{reco}}, E_{\text{true}}\right) \frac{\mathrm{d}\Phi\left(E_{\text{true}}\right)}{\mathrm{d}E_{\text{true}}} P(E_{\text{true}},\Theta)\sigma_{\text{CC}}\left(E_{\text{true}}\right)\epsilon\left(E_{\text{true}}\right) \\ &+\eta_b N_{bi}\end{aligned} \tag{2.10}$$

where

- E_{reco} is the reconstructed neutrino energy.
- E_{true} is the true neutrino energy.
- $f_{\text{res}}\left(E_{\text{reco}}, E_{\text{true}}\right)$ is the probability to observe a reconstructed energy E_{reco} if the true energy is E_{true}. This function is usually taken to be a Gaussian centred at $E_{\text{reco}} = E_{\text{true}}$ with a standard deviation $E_{\text{true}}\sigma_E$, being σ_E the energy resolution of the detector. This functional form stems from assuming $\frac{E_{\text{true}}-E_{\text{reco}}}{E_{\text{true}}}$ to be Gaussian-distributed around 0 with a standard deviation σ_E.
- $\frac{\mathrm{d}\Phi(E_{\text{true}})}{\mathrm{d}E_{\text{true}}}$ is the incident neutrino flux.
- $P(E_{\text{true}},\Theta)$ is the oscillation probability from the original neutrino flavour to the detected flavour.
- $\sigma_{\text{CC}}\left(E_{\text{true}}\right)$ is the neutrino charged current interaction cross section with the detector. At the energies of NOνA both quasi-elastic processes, in which the neutrino scatters off a nucleon that remains intact, and inelastic processes, where nucleons are broken, dominate. In particular, Fig. 2.3 shows the cross section per target nucleon for different processes as a function of the energy.

- $\epsilon\left(E_{\text{true}}\right)$ is the detection efficiency, i.e., the probability to correctly detect, reconstruct and identify a neutrino with energy E_{true}. It is an arbitrarily complicated function that takes into account not only the efficiency of the detector but also the analysis process.

- N_{bi} is the number of background events in the bin.

In other words, the average number of signal events is, without considering experimental effects, the product of incident flux $\frac{\mathrm{d}\Phi}{\mathrm{d}E}$, oscillation probability P, and interaction cross section σ_{CC}. The experimental process introduces a detection efficiency ϵ, a reconstructed average energy $\int_0^\infty \mathrm{d}E_{\text{true}} f_{\text{res}}\left(E_{\text{reco}}, E_{\text{true}}\right)$, and energy bins $\int_{E_i}^{E_{i+1}} \mathrm{d}E_{\text{reco}}$. Background events N_{bi} are added to μ_i. Finally, systematic uncertainties modify the total number of signal and background events as well as the absolute reconstructed energy scale.

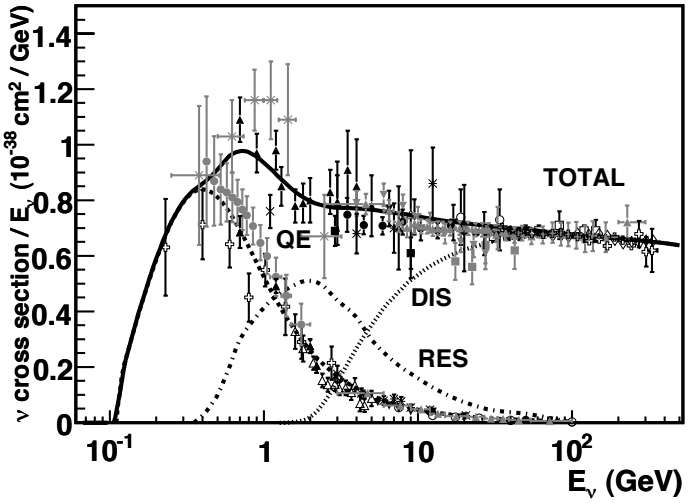

Figure 2.3: Neutrino charged current interaction cross section per target nucleon divided by the neutrino energy for different channels as a function of the neutrino energy. Different data points correspond to different experiments. Source: Ref. [50]

Evaluating Eq. (2.10) allows to reproduce the NOνA statistical analyses. From a practical point of view, the integration over E_{reco} was done analytically due to the Gaussian distribution of $f_{\text{res}}\left(E_{\text{reco}}, E_{\text{true}}\right)$. The integration over E_{true}, on the other hand, was done numerically using an adaptive Gaussian quadrature algorithm [51]. All the minimisations required for calculating χ^2 were done numerically using the `Minuit` library [52].

2.2.2 Muon neutrino disappearance

The NOνA muon neutrino disappearance results, published in Ref. [11], look for muon neutrino events in the far detector. That is, they are sensitive to the muon neutrino survival probability [53]

$$P\left(\nu_\mu \to \nu_\mu\right) = 1 - \sin^2\left(2\theta_{\text{eff}}\right)\sin^2\left(\frac{\Delta m^2_{\text{eff}} L}{4E}\right) + \mathcal{O}\left(\frac{\Delta m^2_{21} L}{E}\right)^3 , \tag{2.11}$$

with

$$\sin^2\left(2\theta_{\text{eff}}\right) = 4\sin^2\theta_{23}\cos^2\theta_{13}\left(1 - \sin^2\theta_{23}\cos^2\theta_{13}\right) \simeq \sin^2\left(2\theta_{23}\right) , \tag{2.12}$$

$$\Delta m^2_{\text{eff}} = \Delta m^2_{32} + \Delta m^2_{21}\sin^2\theta_{12} + \Delta m^2_{21}\cos\delta_{\text{CP}}\sin\theta_{13}\tan\theta_{23}\sin 2\theta_{12} \simeq \Delta m^2_{32} . \tag{2.13}$$

By measuring the total amount of events θ_{23} can be obtained, whereas the energy spectrum allows to measure $|\Delta m^2_{32}|$. This equation takes essentially the form of a vacuum two-neutrino oscillation probability (1.15) with $\theta \simeq \theta_{23}$ and $\Delta m^2 \simeq \Delta m^2_{32}$, so there is very little sensitivity to the mass ordering and the θ_{23} octant.

Getting to the results of the official NOνA analysis, the predicted and measured energy spectrum with and without oscillations is depicted in Fig. 2.4. A full statistical analysis led to the 90% CL contour in Fig. 2.5, where all the other oscillation parameters had been set to the ones in Ref. [18] and normal ordering had been assumed. For future reference, the oscillation parameters in Ref. [18] are

$$\begin{aligned} &\sin^2(2\theta_{12}) = 0.846 \pm 0.021 && \Delta m^2_{21} = (7.53 \pm 0.18) \times 10^{-5}\ \text{eV}^2 \\ &\sin^2(2\theta_{23}) = \begin{cases} 0.999^{+0.001}_{-0.018} & \text{for NO} \\ 1.000^{+0.000}_{-0.017} & \text{for IO} \end{cases} && \Delta m^2_{32} = \begin{cases} (2.44 \pm 0.06)10^{-}3\ \text{eV}^2 & \text{for NO} \\ -(2.52 \pm 0.07)10^{-3}\ \text{eV}^2 & \text{for IO} \end{cases} \\ &\sin^2(2\theta_{13}) = 0.093 \pm 0.008 \end{aligned} \tag{2.14}$$

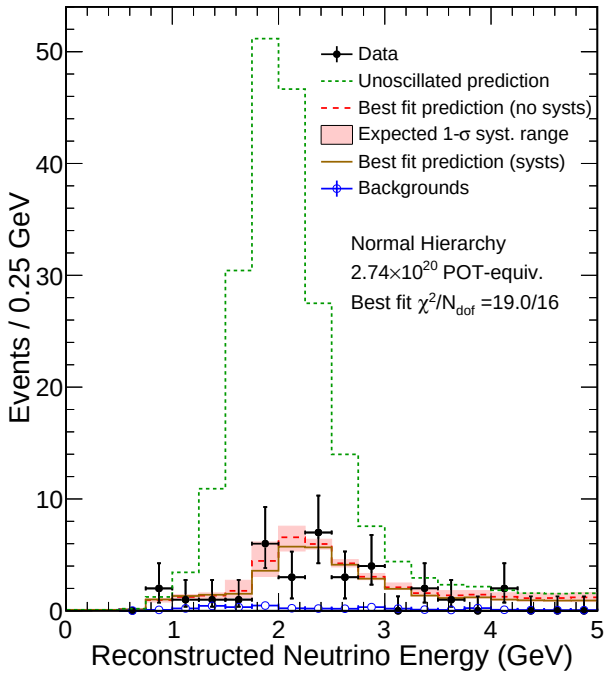

Figure 2.4: Muon neutrino disappearance spectrum. "Best fit prediction" refers to the prediction assuming $\sin^2\theta_{23} = 0.43$ and $\Delta m^2_{32} = 2.52 \cdot 10^{-3}\text{eV}^2$. Figure taken from Ref. [11]

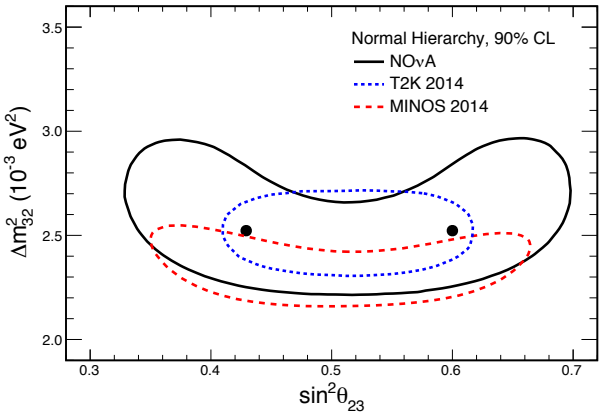

Figure 2.5: 90% confidence level contour in $\left(\Delta m^2_{32}, \sin^2\theta_{23}\right)$ space along with the (degenerate) best fit. Figure taken from Ref. [11].

In order to correctly replicate these results, predictions for the data in Fig. 2.4 have to be

generated for different values of the oscillation parameters and apply the procedure described in the previous section. The predictions are in principle given by Eq. (2.10), where

- $\left(\frac{\mathrm{d}\Phi}{\mathrm{d}E_{\mathrm{true}}}\sigma_{\mathrm{CC}}\epsilon\right)(E_{\mathrm{true}})$ can be obtained from information published by the NOνA collaboration, as sketched in Fig. 2.6. The result is then correctly normalised bin-per-bin by setting the oscillation probability to 1 and comparing the results with the unoscillated prediction in Fig. 2.4.
- N_{bi} can be read from Fig. 2.4.
- The full oscillation probability including matter effects is considered, assuming the Earth crust to have a constant density of 2.76 g/cm^3 and matter with the same number of protons and neutrons [46].
- All the other parameters in Eq. (2.10) have been given in Sec. 2.1.3 .

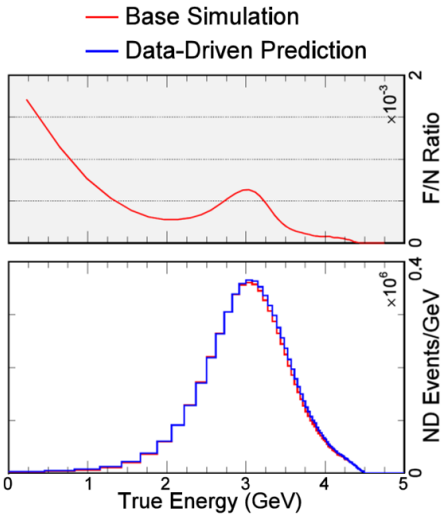

Figure 2.6: Data-driven simulation of the near detector flux (below, blue) and far-to-near detector ratio (above) as a function of true energy. Interpolating the bottom curve and multiplying it by the top one gives $\left(\frac{\mathrm{d}\Phi}{\mathrm{d}E_{\mathrm{true}}}\sigma_{\mathrm{CC}}\epsilon\right)(E_{\mathrm{true}})$. Plots extracted from Ref. [45].

Finally, as in the original NOνA analysis, all the oscillation parameters except for Δm^2_{32} and $\sin^2\theta_{23}$ are treated as Gaussian-distributed nuisance parameters with means and standard deviations given by Ref. [18] (see Eq. (2.14)).

The resulting confidence contours, depicted in Fig. 2.7, are in reasonable qualitative agreement with the official NOνA result. The spectrum at the best fit, shown in Fig. 2.8, has also the expected qualitative shape. However, the quantitative agreement was considered not to be good enough.

The observed differences between the presented simulation and the NOνA results might be related to the naive way of treating systematic uncertainties in Eq. (2.10). In particular, as mentioned in Sec. 2.1.3, NOνA reported a large discrepancy between data and simulation in the energy deposited by hadrons in the detector. That systematic uncertainty, the largest one they had, is introduced at a low level in the simulation of the process, so it is hard to reproduce it in this analysis.

In order to deal with that, the approach to systematic uncertainties was completely modified: all the systematic uncertainty shifts in Fig. 2.4 are now assumed to be fully correlated among them, controlled by a single, energy-independent, Gaussian distributed parameter ξ. Quantitatively, let μ^i_{up} and μ^i_{low} be the upper and lower bounds of the 1-σ systematic range in Fig. 2.4 and let $\mu^i_{\mathrm{no\ sys}}$ be the predictions without systematics in the same figure. Assuming that all

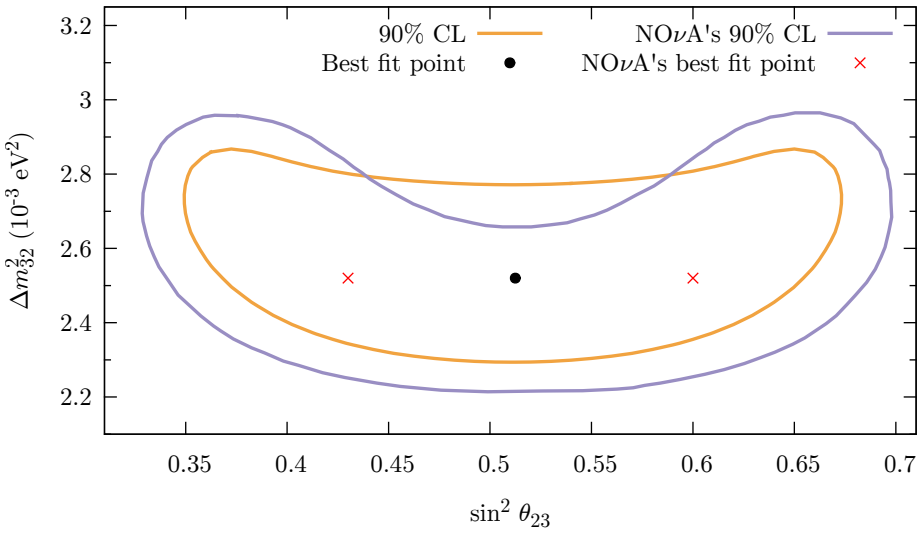

Figure 2.7: First attempt to reproduce the NOνA contour. The 90% CL contour assumes Gaussian regime in χ^2, whereas NOνA used a Monte Carlo simulation that according to Ref. [48] does not appreciably change the result.

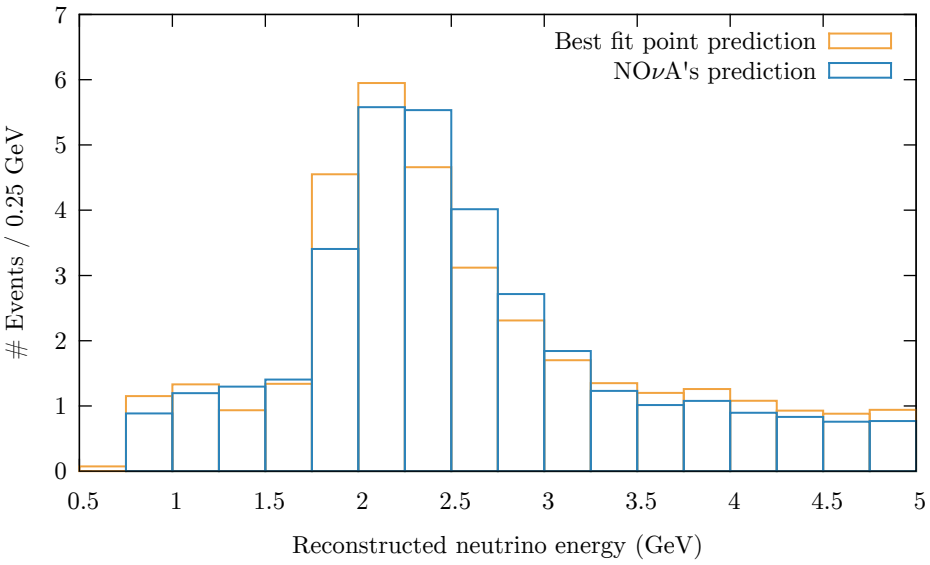

Figure 2.8: Spectrum at the best fit obtained in the first attempt to reproduce the NOνA contour.

systematic uncertainties can be parametrised by a single additive term, the prediction for each μ_i changes to

$$\mu_i = \begin{cases} \mu_i^0 + \xi \left(\mu^i_{\text{up}} - \mu^i_{\text{no sys}}\right) & \text{if } \xi > 0 \\ \mu_i^0 + \xi \left(\mu^i_{\text{no sys}} - \mu^i_{\text{low}}\right) & \text{if } \xi < 0 \end{cases}, \tag{2.15}$$

where μ_i^0 is the result of Eq. (2.10) with all systematic parameters set to 1. ξ is then Gaussian distributed around 0 with standard deviation 1.

With that treatment of systematic uncertainties, the contour in Fig. 2.9 is obtained, which matches much better the official one. What is more, the best fit spectrum, Fig. 2.10, essentially matches the official result.

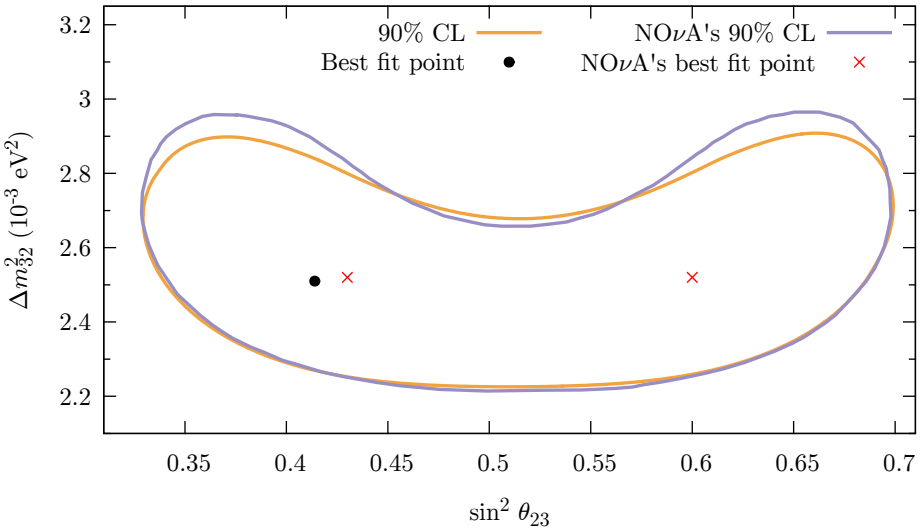

Figure 2.9: NOνA contour generated assuming a single systematic parameter. NOνA's best fit points and the obtained one differ in $\Delta\chi^2 \lesssim 0.08$. The θ_{23} octant degeneracy is very slightly broken by matter effects.

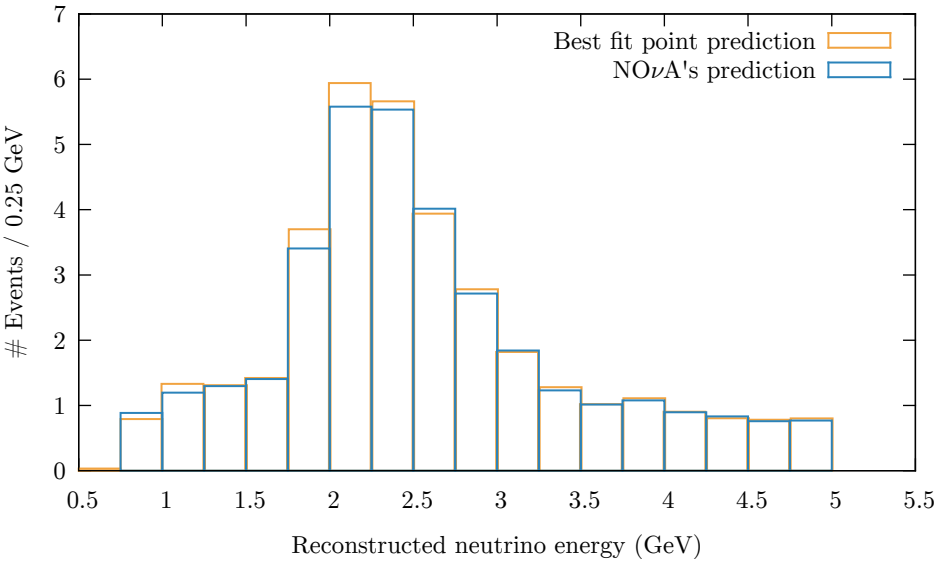

Figure 2.10: NOνA best-fit spectrum generated assuming a single systematic parameter.

2.2.3 Electron neutrino appearance

The NOνA experiment was particularly designed to measure the process $\nu_\mu \to \nu_e$, and its first results were published in Ref. [12]. As mentioned in Sec. 1.2, the relevant oscillation probability can be approximated in constant matter by:

$$\begin{aligned} P\left(\nu_\mu \to \nu_e\right) = & \sin^2\theta_{23}\sin^2 2\theta_{13}\frac{\sin^2\Delta(1-A)}{(1-A)^2} \\ & + \frac{\Delta m^2_{21}}{\Delta m^2_{31}}\cos\theta_{13}\sin 2\theta_{13}\sin 2\theta_{12}\sin 2\theta_{23}\cos\left(\Delta+\delta_{\text{CP}}\right)\frac{\sin\Delta A}{A}\frac{\sin\Delta(1-A)}{(1-A)} \\ & + \left(\frac{\Delta m^2_{21}}{\Delta m^2_{31}}\right)^2\cos^2\theta_{23}\sin^2 2\theta_{12}\frac{\sin^2\Delta A}{A^2} + \mathcal{O}\left(\frac{\Delta m^2_{21}}{\Delta m^2_{31}}\right)^3, \end{aligned} \tag{2.16}$$

where $\Delta \equiv \Delta m^2_{31}\frac{L}{4E}$, $A = 2\sqrt{2}G_F n_e \frac{E}{\Delta m^2_{31}}$, and n_e is the electron number density in the Earth matter travelled by neutrinos. This process yields dominant information on δ_{CP} and θ_{13}.

Getting to the particular results, Fig. 2.11 shows the predicted and observed electron neutrino spectrum. Figure 2.12, on the other hand, shows the 68% and 90% CL on $\sin^2 2\theta_{13}$ for different values of δ_{CP}, treating the other oscillation parameters as Gaussian-distributed nuisance parameters with means and standard deviations given by Ref. [18] (see Eq. (2.14)). The fit employs the total amount of data, without dividing the events in energy bins [46]. In all cases, both selection techniques mentioned in Sec. 2.1.3 are considered, LEM providing more data and including the events selected by LID.

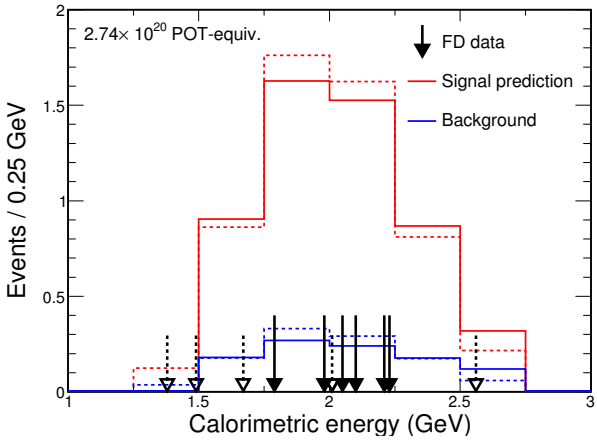

Figure 2.11: Electron neutrino appearance spectrum. Solid arrows show the data using the LID selector, whereas the LEM selector data includes both solid and dashed arrows. Solid predictions correspond to the LID selector, and dashed predictions to the LEM selector; in all cases they are generated using $\sin^2\theta_{23} = 0.5$, $\Delta m^2_{32} = 2.37{\cdot}10^{-3}$ eV^2, $\sin^2 2\theta_{12} = 0.846$, $\Delta m^2_{21} = 7.53{\cdot}10^{-5}$ eV^2, $\sin^2 2\theta_{13} = 0.086$, and $\delta_{\text{CP}} = 0$. Figure taken from Ref. [12].

In principle, to replicate these results the same procedure first used in the muon analysis, with 3 independent systematic uncertainties, could be followed. Nevertheless, as far as the author of this work is aware, NOνA has not released information about $\left(\frac{\mathrm{d}\Phi}{\mathrm{d}E_{\text{true}}}\sigma_{\text{CC}}\epsilon\right)(E_{\text{true}})$ for electron neutrinos. In order to deal with this, first the predictions in Fig. 2.11 assuming the value of $\left(\frac{\mathrm{d}\Phi}{\mathrm{d}E_{\text{true}}}\sigma_{\text{CC}}\epsilon\right)$ for muon neutrinos are generated. The results are then normalised bin-per-bin to the ones in Fig. 2.11, thus assuming the ratio of $\sigma_{\text{CC}}\epsilon$ between electron and muon neutrinos to be constant within each energy bin. The obtained normalisation parameters do not significantly depend on the bin, showing the validity of the procedure. What is more, since as mentioned the analysis does not divide the data in energy bins, energy-dependent effects are not very significant.

Besides, since 50% of the background consists of electron neutrinos from the beam with an essentially flat energy distribution [54], half of the background is also modified when changing the oscillation parameters. Finally, as in the NOνA analysis, all the oscillation parameters except for

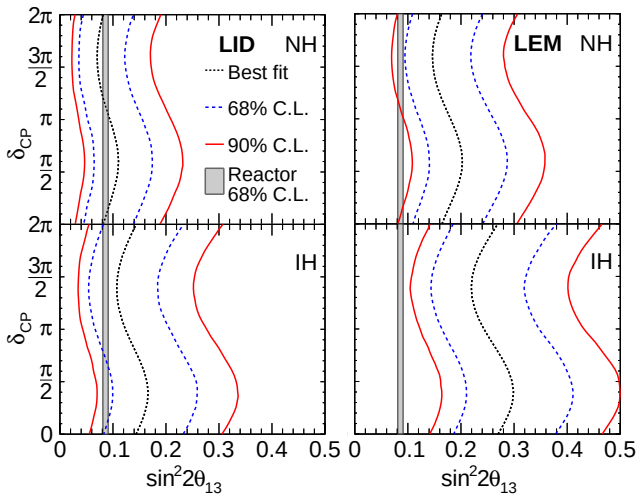

Figure 2.12: Confidence levels on $\sin^2 2\theta_{13}$ for different δ_{CP}, different selection techniques, and different mass orderings (NH refers to normal ordering and IH to inverted ordering). The vertical grey band corresponds to the independent 1σ range of θ_{13} from reactor experiments (see Eq. (2.14)). As will be discussed in the next chapter, this discrepancy between that range and the NOνA best fit for some figures has quantitative effects when statistically combining NOνA with other experiments. Figure taken from Ref. [12].

δ_{CP} and θ_{13} are treated as Gaussian-distributed nuisance parameters with means and standard deviations extracted from Ref. [18] (see Eq. (2.14)).

The resulting confidence contours are shown in Fig. 2.13. As it is seen, the results accurately match the official NOνA ones, where the small differences for large $\sin^2 2\theta_{13}$ may stem from NOνA calculating the contours with a Monte Carlo simulation while this analysis uses the Gaussian approximation. In Ref. [46], a comparison of the regions using both methods (but with a smaller data sample) is presented. The comparison indicates that using the Monte Carlo defined CLs would slightly extend the right edge of the contours, matching better the ones of the NOνA analysis.

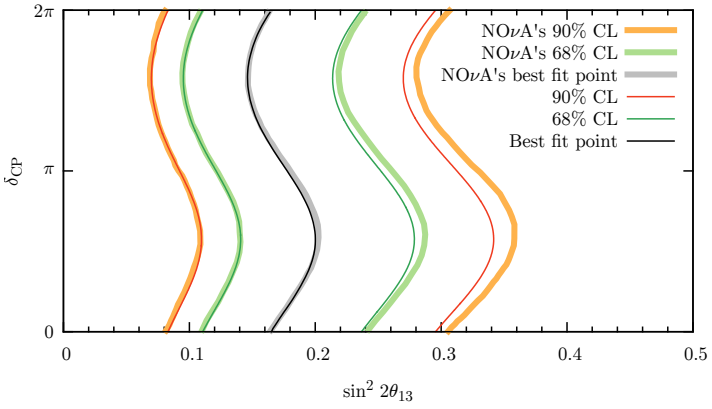

(a) LEM selection technique, normal ordering.

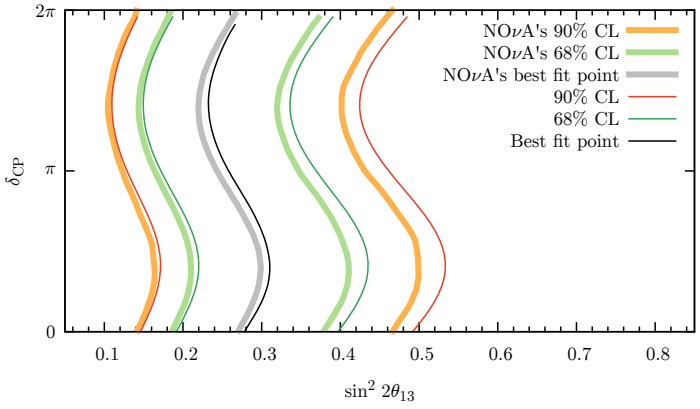

(b) LEM selection technique, inverted ordering.

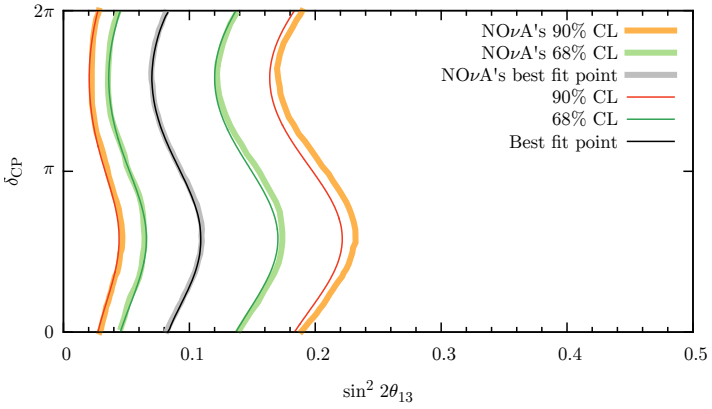

(c) LID selection technique, normal ordering.

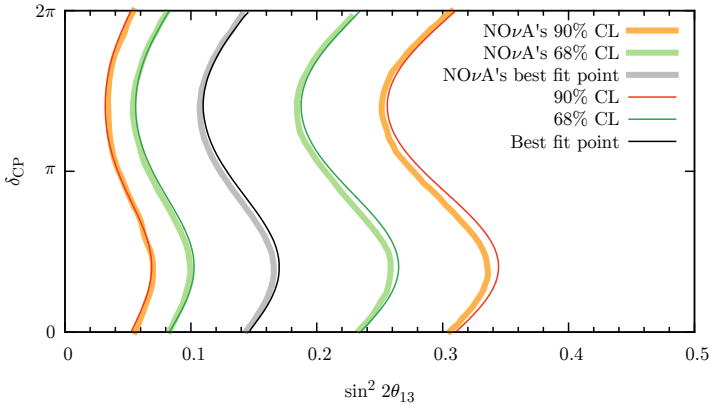

(d) LID selection technique, inverted ordering.

Figure 2.13: Resulting contours for NOνA electron neutrino appearance analysis. Gaussian regime for χ^2 is assumed. The best-fit discrepancies for IO are small, $\Delta\chi^2 \lesssim 0.02$.

Chapter 3

Combination of NOνA data with other experiments

Once a procedure for calculating χ^2 for NOνA has been established and checked against official results from the collaboration, it is straightforward to combine it with previous results from the NuFIT group [3] and obtain an up-to-date global fit of neutrino oscillation parameters. Moreover, dedicated analyses to determine the current statistical confidence on δ_{CP} and/or the mass ordering can also be run.

3.1 Global analysis

After combining the NOνA results with the ones in Ref. [3] as well as data from the DeepCore experiment and new samples from the T2K experiment, the global fit presented in Sec. 1.2.2 was updated and the result was made publicly available [1]. The new best fit parameters are shown in Table 3.1, whereas Fig. 3.1 shows the correlations between the variables in which the NOνA data had the largest impact.

To address more in detail the impact of including the NOνA results, Fig. 3.2 shows $\Delta\chi^2$ as a function of either Δm^2_{32}, $\sin^2\theta_{23}$, or δ_{CP} with and without the new additions. As the figure shows, when using the results of the analysis carried out with the LID selection procedure, including NOνA data does not introduce any dramatic change, mostly confirming previously existing tendencies. Using the results obtained with the LEM selection procedure, on the other hand, has some impact on the three worse-known properties of neutrino mixing:

- The preferred mass ordering changes from IO to NO, as the figures on the first line in Fig. 3.2 show (see below for a possible explanation).
- NOνA LEM data favours $\theta_{23} > 45°$ (see below for a possible explanation) and, as a consequence, the significance of the θ_{23} octant is affected. For IO this confirms the previous tendency. For NO, on the other hand, including NOνA LEM changes the favoured octant from the first to the second. The previous favouring of the first octant in NO was mostly driven by atmospheric neutrino data, which shows an excess of sub-GeV events that for NO was accommodated by $\theta_{23} < 45°$ [3]. Inclusion of NOνA LEM results conflicts with this tendency.
- The $\Delta\chi^2$ distributions for δ_{CP} are also significantly affected, particularly for IO. The smaller impact that including NOνA LEM has for NO is also a consequence of the change of the favoured θ_{23} octant for that mass ordering: as Fig. 3.1 shows, the second octant, now favoured, has a lower significance on δ_{CP}.

The effect that NOνA LEM results have on θ_{23} can be understood from Fig. 2.12 (right): there seems to be tension between the independently measured value of θ_{13} and the one determined one NOνA in ν_e appearance. As Eq. (2.16) shows, however, the ν_e appearance probability is mostly sensitive not to θ_{13} but to the combination $\sin^2\theta_{23}\sin^2 2\theta_{13}$. The official NO$\nu$A analysis

LEM	Normal Ordering (best fit) bfp $\pm1\sigma$	Normal Ordering (best fit) 3σ range	Inverted Ordering ($\Delta\chi^2 = 0.97$) bfp $\pm1\sigma$	Inverted Ordering ($\Delta\chi^2 = 0.97$) 3σ range	Any Ordering 3σ range
$\sin^2\theta_{12}$	$0.308^{+0.013}_{-0.012}$	$0.273 \to 0.349$	$0.308^{+0.013}_{-0.012}$	$0.273 \to 0.349$	$0.273 \to 0.349$
$\theta_{12}/^\circ$	$33.72^{+0.79}_{-0.76}$	$31.52 \to 36.18$	$33.72^{+0.79}_{-0.76}$	$31.52 \to 36.19$	$31.52 \to 36.18$
$\sin^2\theta_{23}$	$0.574^{+0.026}_{-0.144}$	$0.390 \to 0.639$	$0.579^{+0.022}_{-0.029}$	$0.400 \to 0.637$	$0.390 \to 0.639$
$\theta_{23}/^\circ$	$49.3^{+1.5}_{-8.3}$	$38.6 \to 53.1$	$49.6^{+1.3}_{-1.7}$	$39.2 \to 53.0$	$38.6 \to 53.1$
$\sin^2\theta_{13}$	$0.0217^{+0.0013}_{-0.0010}$	$0.0187 \to 0.0250$	$0.0221^{+0.0010}_{-0.0010}$	$0.0190 \to 0.0251$	$0.0187 \to 0.0250$
$\theta_{13}/^\circ$	$8.47^{+0.24}_{-0.20}$	$7.86 \to 9.11$	$8.54^{+0.19}_{-0.20}$	$7.93 \to 9.12$	$7.86 \to 9.11$
$\delta_{\rm CP}/^\circ$	272^{+61}_{-64}	$0 \to 360$	256^{+43}_{-43}	$131 \to 381$	$0 \to 360$
$\frac{\Delta m^2_{21}}{10^{-5}\ \text{eV}^2}$	$7.49^{+0.19}_{-0.17}$	$7.02 \to 8.08$	$7.49^{+0.19}_{-0.17}$	$7.02 \to 8.08$	$7.02 \to 8.08$
$\frac{\Delta m^2_{3\ell}}{10^{-3}\ \text{eV}^2}$	$+2.484^{+0.045}_{-0.048}$	$+2.351 \to +2.618$	$-2.467^{+0.041}_{-0.042}$	$-2.595 \to -2.341$	$\begin{bmatrix}+2.325 \to +2.618\\ -2.588 \to -2.348\end{bmatrix}$
LID	Normal Ordering ($\Delta\chi^2 = 1.03$) bfp $\pm1\sigma$	Normal Ordering ($\Delta\chi^2 = 1.03$) 3σ range	Inverted Ordering (best fit) bfp $\pm1\sigma$	Inverted Ordering (best fit) 3σ range	Any Ordering 3σ range
$\sin^2\theta_{12}$	$0.308^{+0.013}_{-0.012}$	$0.273 \to 0.349$	$0.308^{+0.013}_{-0.012}$	$0.273 \to 0.349$	$0.273 \to 0.349$
$\theta_{12}/^\circ$	$33.72^{+0.79}_{-0.76}$	$31.52 \to 36.18$	$33.72^{+0.79}_{-0.76}$	$31.52 \to 36.18$	$31.52 \to 36.18$
$\sin^2\theta_{23}$	$0.451^{+0.038}_{-0.025}$	$0.387 \to 0.634$	$0.576^{+0.023}_{-0.033}$	$0.393 \to 0.636$	$0.389 \to 0.636$
$\theta_{23}/^\circ$	$42.2^{+2.2}_{-1.4}$	$38.5 \to 52.8$	$49.3^{+1.4}_{-1.9}$	$38.8 \to 52.9$	$38.6 \to 52.9$
$\sin^2\theta_{13}$	$0.0219^{+0.0010}_{-0.0010}$	$0.0188 \to 0.0249$	$0.0219^{+0.0010}_{-0.0010}$	$0.0189 \to 0.0250$	$0.0189 \to 0.0250$
$\theta_{13}/^\circ$	$8.50^{+0.19}_{-0.20}$	$7.87 \to 9.08$	$8.51^{+0.20}_{-0.20}$	$7.89 \to 9.10$	$7.89 \to 9.10$
$\delta_{\rm CP}/^\circ$	303^{+39}_{-50}	$0 \to 360$	262^{+51}_{-57}	$98 \to 416$	$0 \to 360$
$\frac{\Delta m^2_{21}}{10^{-5}\ \text{eV}^2}$	$7.49^{+0.19}_{-0.17}$	$7.02 \to 8.08$	$7.49^{+0.19}_{-0.17}$	$7.02 \to 8.08$	$7.02 \to 8.08$
$\frac{\Delta m^2_{3\ell}}{10^{-3}\ \text{eV}^2}$	$+2.477^{+0.042}_{-0.042}$	$+2.351 \to +2.610$	$-2.465^{+0.041}_{-0.043}$	$-2.594 \to -2.339$	$\begin{bmatrix}+2.355 \to +2.606\\ -2.594 \to -2.339\end{bmatrix}$

Table 3.1: Results of global fit to neutrino oscillation parameters as of May 2016. "bfp" stands for best fit point. $\Delta m^2_{3\ell}$ refers to Δm^2_{31} for NO and Δm^2_{32} for IO. Source: Ref [1].

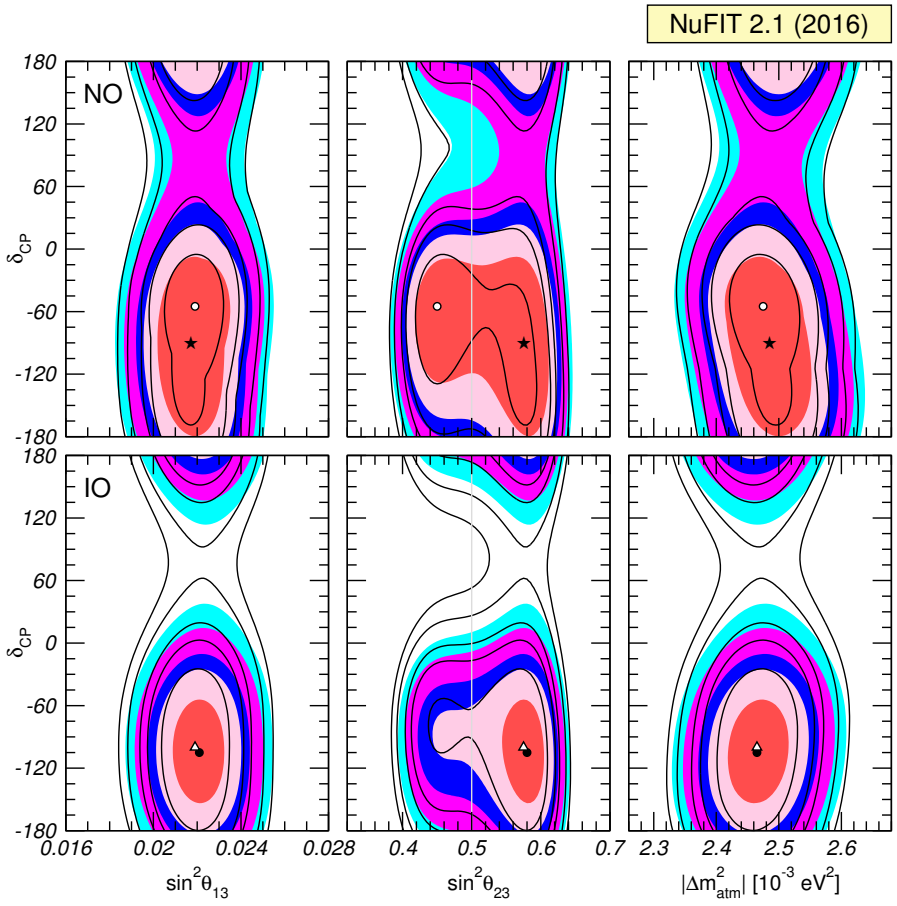

Figure 3.1: Correlation between $\delta_{\rm CP}$ and θ_{13} or θ_{23} or $\Delta m^2_{3\ell}$ for different mass orderings. Each panel shows the two-dimensional projection of the allowed six-dimensional region after marginalisation with respect to the undisplayed parameters. The different contours correspond to the two-dimensional allowed regions at 1σ, 90%, 2σ, 99%, 3σ CL. The points correspond to the best fit. For the same panel, black best fit and contours correspond to the NOνA LID selection procedure, whereas coloured contours and white best fit correspond to the LEM selection procedure. Source: Ref [1].

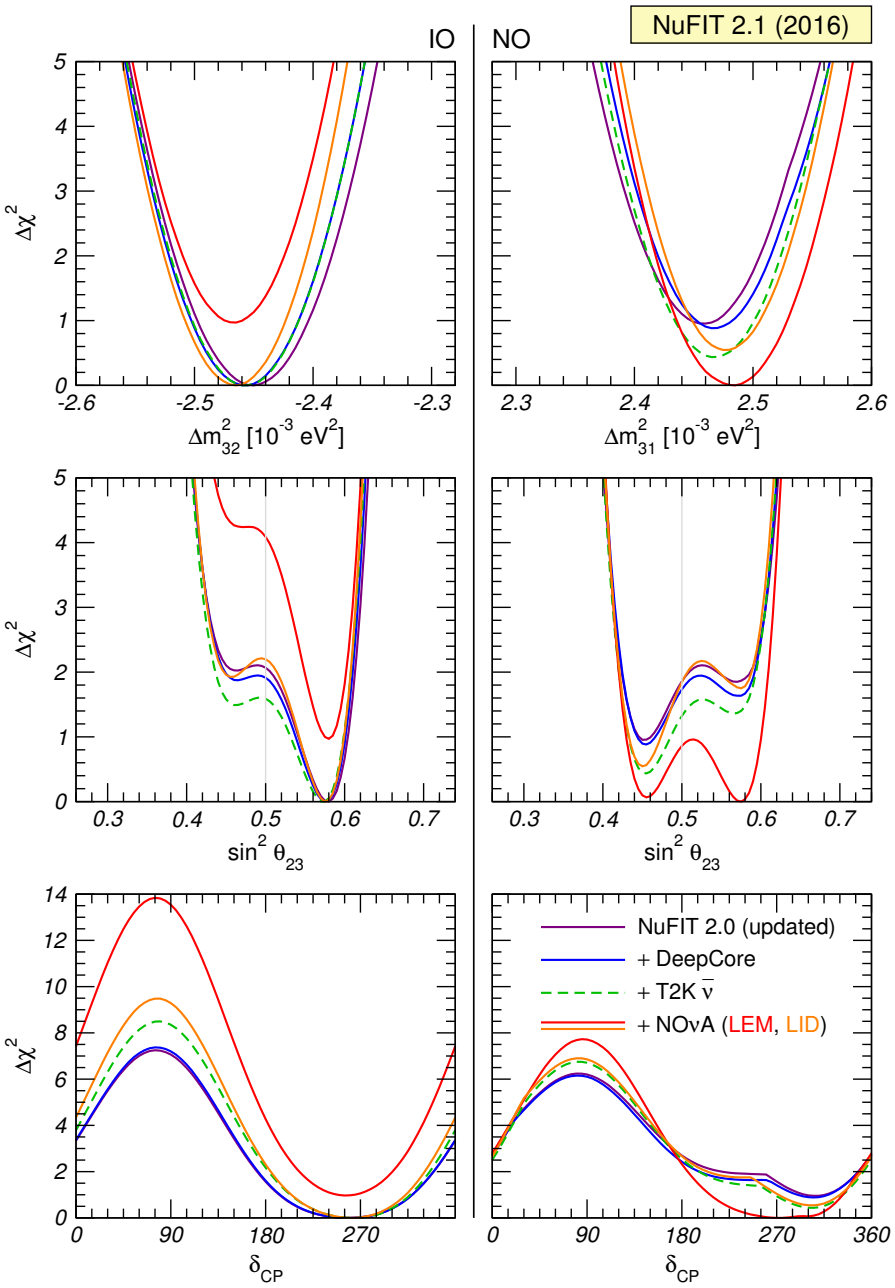

Figure 3.2: $\Delta\chi^2$ distribution for different oscillation parameters as a result of adding different experiments. In each plot, χ^2 is minimised with respect to all other oscillation parameters except for the mass ordering: the plots are 1-dimensional $\Delta\chi^2$ projections. Source: Ref [1].

results shown in in Fig. 2.12 effectively assume $\theta_{23} = 45°$ (see Eq. (2.14)) but a smaller θ_{13} can be equally accommodated if one allows for $\theta_{23} > 45°$.

What is more, as seen in the same figure, the θ_{13} tension between NOνA LEM and reactor experiments is larger for IO. Therefore, this mass ordering requires a larger value of θ_{23} to be consistent with reactor θ_{13} data. But large deviations from $\theta_{23} = 45°$ are disfavoured by ν_μ disappearance data from NOνA, T2K and atmospheric neutrinos. As a consequence, an overall agreement among all data sets becomes more difficult for IO and this mass ordering is disfavoured as a result.

Because of the limited NOνA statistics all these effects do not lead to large values of $\Delta\chi^2$, this is, they are still not very statistically significant. To quantify their impact on the significance of our present knowledge of the CP violating phase and the ordering a numerical study has been carried out to take into account that deviations from Gaussianity can be expected because of the cyclic nature of the CP phase and the discreteness of the ordering, as well due to the limited statistics of the appearance results.

3.2 Present significance of mass ordering and CP violation

3.2.1 Test statistic

The mass ordering and CP violation phase $\delta_{\rm CP}$ are among the less-known neutrino mixing parameters. Since NOνA data affects both, to quantify the current statistical knowledge on them the following test statistic is considered:

$$\Delta\chi^2\left(\delta_{\rm CP}, \text{ord}\right) = \chi^2\left(\delta_{\rm CP}, \text{ord}\right) - \min_{\delta_{\rm CP}, \text{ord}} \chi^2\left(\delta_{\rm CP}, \text{ord}\right) \tag{3.1}$$

where ord refers to the mass ordering. It is the natural extension of the test statistic (2.4) if just $\delta_{\rm CP}$ and the mass ordering are to be studied.

With respect to the other oscillation parameters, $\sin^2\theta_{23}$ and $|\Delta m^2_{32}|$ are strongly correlated with $\delta_{\rm CP}$, as Fig. 3.1 shows. Therefore, χ^2 must be minimised over them, i.e.,

$$\chi^2\left(\delta_{\rm CP}, \text{ord}\right) = \min_{\sin^2\theta_{23}, |\Delta m^2_{32}|} \chi^2\left(\delta_{\rm CP}, \text{ord}, \sin^2\theta_{23}, |\Delta m^2_{32}|\right) . \tag{3.2}$$

On the other hand, the oscillation parameters $\sin^2\theta_{12}$, $\sin^2\theta_{13}$ and Δm^2_{21} are known with a high precision and minimising over them is expected to have a small effect in the test statistic (3.2). What is more, $\sin^2\theta_{12}$ and Δm^2_{21} are determined in experiments different from the ones measuring $\delta_{\rm CP}$ and the mass ordering: being essentially uncorrelated with these parameters, they can safely be kept fixed. Something similar happens with θ_{13}: as Fig. 3.1 shows, the correlation with, e.g., $\delta_{\rm CP}$, is rather small. Thus they are are kept fixed to 0.308, 0.022 and $7.49 \cdot 10^{-5}$ eV^2, respectively.

3.2.2 Confidence levels

In principle Wilk's theorem assures that the test statistic (3.1) is, in the large sample limit, distributed following a χ^2 distribution. The theorem, however, assumes the theoretical predictions to depend linearly on the fit parameters, which can take any real value. This is not strictly true here due to the complicated dependence of the predictions on $\delta_{\rm CP}$ and the mass ordering (see Eq. (1.26)), as well as due to the discreteness of the ordering and the periodicity of $\delta_{\rm CP}$ [55]. Therefore, confidence levels for the test statistic (3.1) have to be obtained with a Monte Carlo simulation to evaluate the real probability distribution followed by the tests statistics used.

Getting into more detail, the systematic uncertainties and data points in the experiments are expected to be, respectively, Gaussian and Poisson distributed. Thus, assuming some "true" values for the oscillation parameters, a set of pseudo-experiments with randomly produced data can be generated. From them, the probability density function distribution of the test statistic (3.1), which will be denoted as $\mathcal{F}(\Delta\chi^2|\delta_{\rm CP}, \text{ord})$, can be estimated. Its dependence on $\delta_{\rm CP}$ and the

mass ordering stems from the dependence on them of the test statistic. Confidence intervals $[0, \Delta\chi^2_\lambda]$ with confidence λ can then be obtained, as in Eq. (2.5), by solving

$$\int_0^{\Delta\chi^2_\lambda} \mathcal{F}(\Delta\chi^2|\delta_{\rm CP}, \text{ord}) = \lambda\,. \tag{3.3}$$

This procedure is equivalent to rejecting $\Delta\chi^2 > \Delta\chi^2_\lambda$ with confidence λ if it occurs in a fraction $1-\lambda$ of the pseudo-experiments. Thus, the confidence intervals have the correct frequentist coverage by construction.

The resulting confidence intervals will in general depend on the "true" values of the oscillation parameters that generate the pseudo-experiments. Since $\Delta\chi^2\left(\delta_{\rm CP}, \text{ord}\right)$ sheds light on the probability of $(\delta_{\rm CP}, \text{ord})$ having generated the data, the "true" values of these parameters should be equal to the ones with which $\Delta\chi^2$ is evaluated. Given the current statistical confidence on other oscillation parameters (see Table 3.1), their "true" values were chosen as $|\Delta m^2_{32}| = 2.4\cdot10^{-3}$ eV^2, $\Delta m^2_{21} = 7.49\cdot10^{-5}$ eV^2, $\sin^2\theta_{12} = 0.308$, and $\sin^2\theta_{13} = 0.022$. As discussed above, as these parameters are independently determined they are very weakly correlated with the CP phase and the ordering. Thus, changing their "true" value is not expected to have much impact on the derived CL. On the contrary, both the CP phase and the ordering show strong correlations with θ_{23} (see Figs. 3.1 and 3.2). For this reason, the analysis is run for three different "true" $\sin^2\theta_{23}$ values: 0.45, 0.58 and 0.5, corresponding, respectively, to the local $\Delta\chi^2$ minima (see Fig. 3.2) and maximal mixing among the 2 and 3 mass eigenstates.

3.2.3 Data sets and results

In order to understand the effect of NOνA data on the confidence on $\delta_{\rm CP}$ and the mass ordering, the test statistic (3.1) and its confidence levels were first evaluated for NOνA data alone, from both ν_μ disappearance and ν_e appearance. Afterwards, the same analysis was run adding data from other accelerator neutrino experiments: T2K (ν_e appearance and ν_μ disappearance data) and MINOS ($\bar\nu_e$ and ν_e appearance and $\bar\nu_\mu$ and ν_μ disappearance data). The base simulations for these two experiments were provided by the NuFIT group.

The resulting data and confidence levels for NOνA, NOνA and T2K, and NOνA, T2K and MINOS are shown in Fig. 3.3 for LEM data, and in Fig. 3.4 for LID data. The confidence levels are extracted from a Monte Carlo (MC) simulation of 10^4 pseudo-experiments.

The results in the figures can be understood as follows. In each panel the values of test statistic 3.1 are plotted for both mass orderings as a function of $\delta_{\rm CP}$ for real experimental data. These are the full red (for NO) and blue (for IO) curves. There are also three red (blue) dashed curves, corresponding to the value $\Delta\chi^2_\lambda$ that determines a λ=68.27%, 90%, and 99 % CL (see Eq. (3.3)). These values are obtained from the MC simulation with "true" NO (IO). If the the test statistics (3.1) was χ^2-distributed (i.e., the Gaussian limit ignoring the discreteness of the ordering), these three curves would be horizontal lines at $\Delta\chi^2_\lambda = 1$, 2.71, and 6.63 for both orderings.

As seen in the figure, in most cases the MC obtained CLs are smaller than the ones expected from the χ^2-approximation, particularly for the larger CLs. Furthermore, there are strong variations on the CL curves for $\theta_{23} \neq 45^\circ$ and the CL curves are always lower for NO than for IO. The first effect can be qualitatively understood in terms of parameter degeneracies in the oscillation probabilities [55], and the fact that the regions with lower CLs are close to the boundaries of the parameter space, thus reducing the effective number of degrees of freedom in the fit and increasing its sensitivity.

The effect on the ordering, on the other hand, shows that the experiments have more sensitivity to reject NO than IO. Its origin may be related to the larger $\nu_\mu \to \nu_e$ oscillation probability for NO than for IO: for NO, the denominator in the first term in Eq. (2.16) is smaller, thus increasing the oscillation probability (this can also be checked evaluating the full oscillation formula). As a consequence, "true" NO predicts more statistics, and thus more sensitivity.

Next, the real $\Delta\chi^2$ values (the full lines) can be compared with the corresponding expected distributions and obtain the CLs. If the real $\Delta\chi^2$ for a given $\delta_{\rm CP}$ and mass ordering is larger than the values obtained for a fraction λ of the pseudo-experiments for that "true" value of

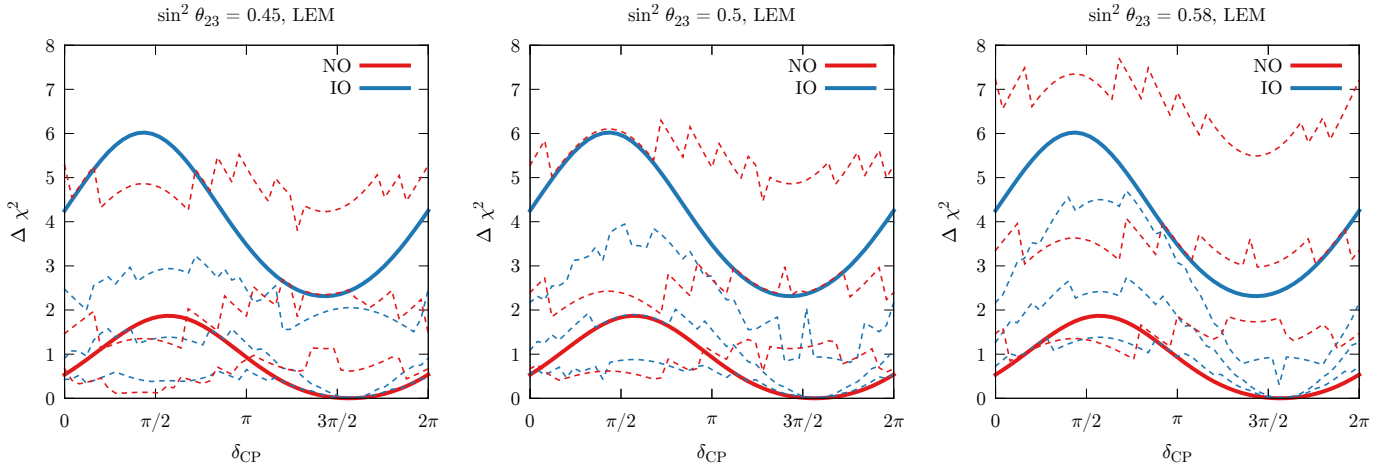

(a) NOνA data

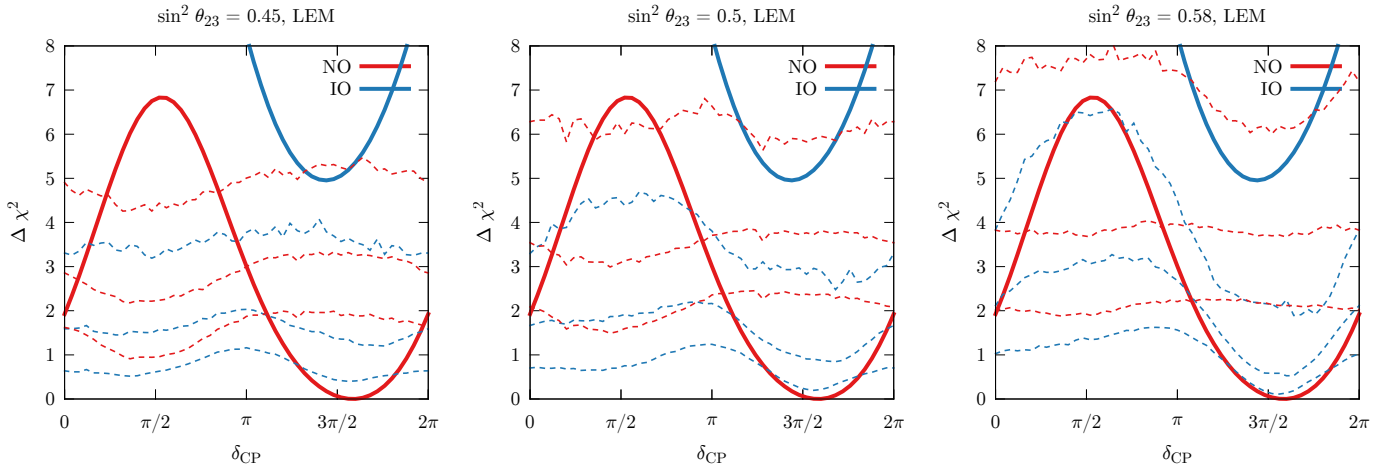

(b) NOνA and T2K data

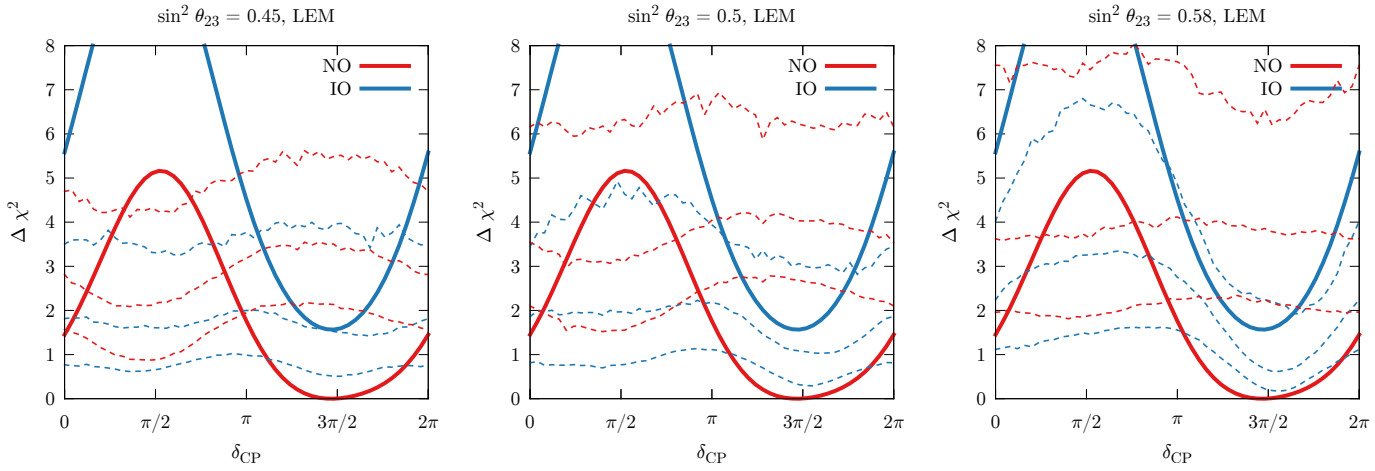

(c) NOνA, T2K and MINOS data

Figure 3.3: Experimental value of the test statistic (3.1) (solid) and its confidence levels (dashed) both for NO (red) and IO (blue) and different "true" θ_{23} values. The dashed lines correspond, from bottom to top, to 68.27%, 90% and 99% CL LEM data. The discrete "steps" present in the NOνA CLs are due to NOνA fitting a single Poisson-distributed discrete variable (the total number of ν_e events) therefore introducing a discretisation in the possible χ^2 values.

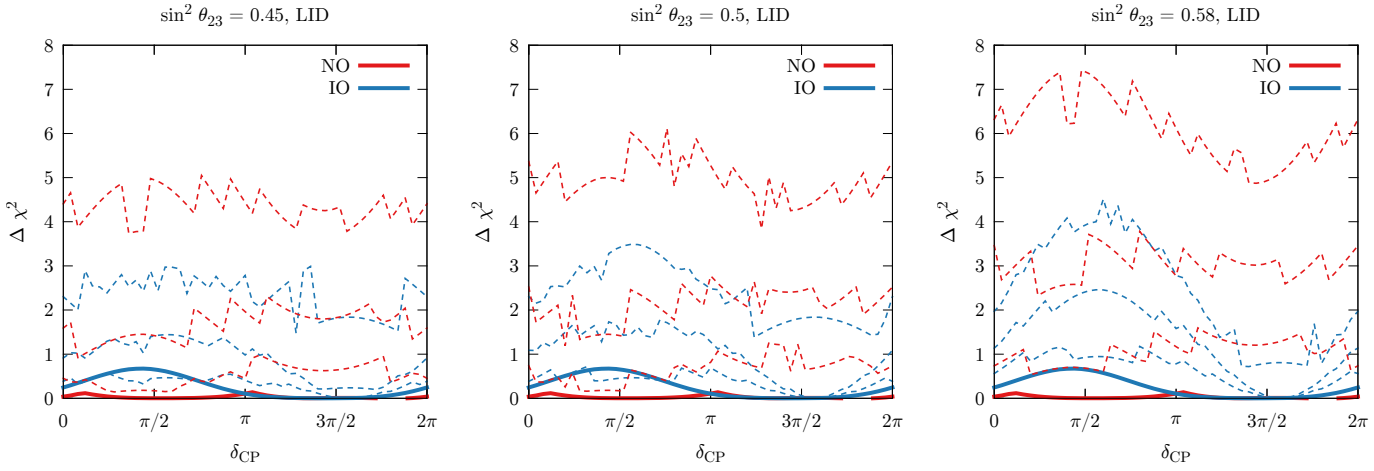

(a) NOνA data

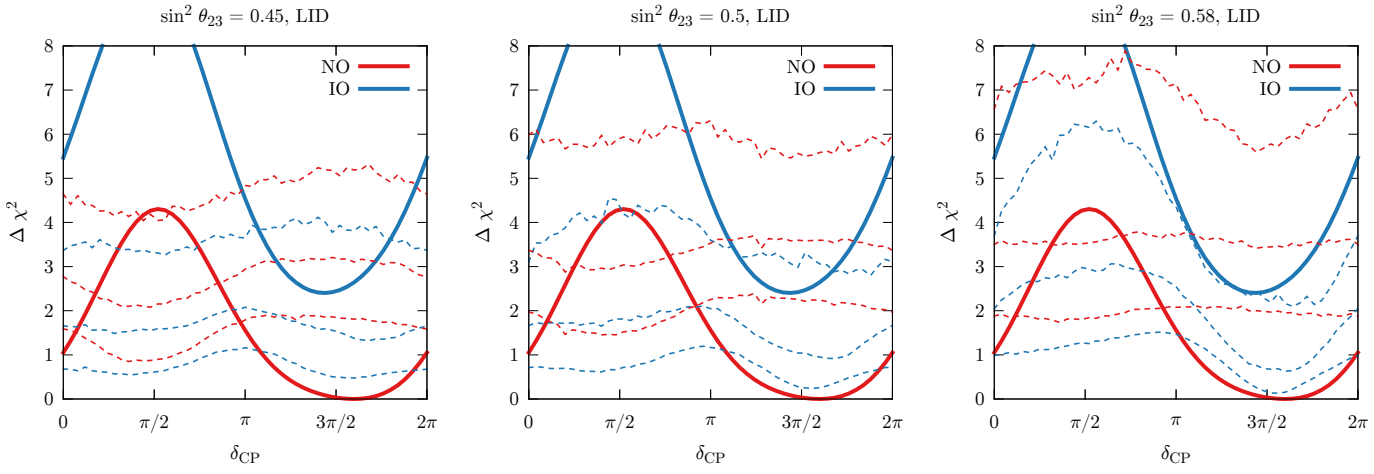

(b) NOνA and T2K data

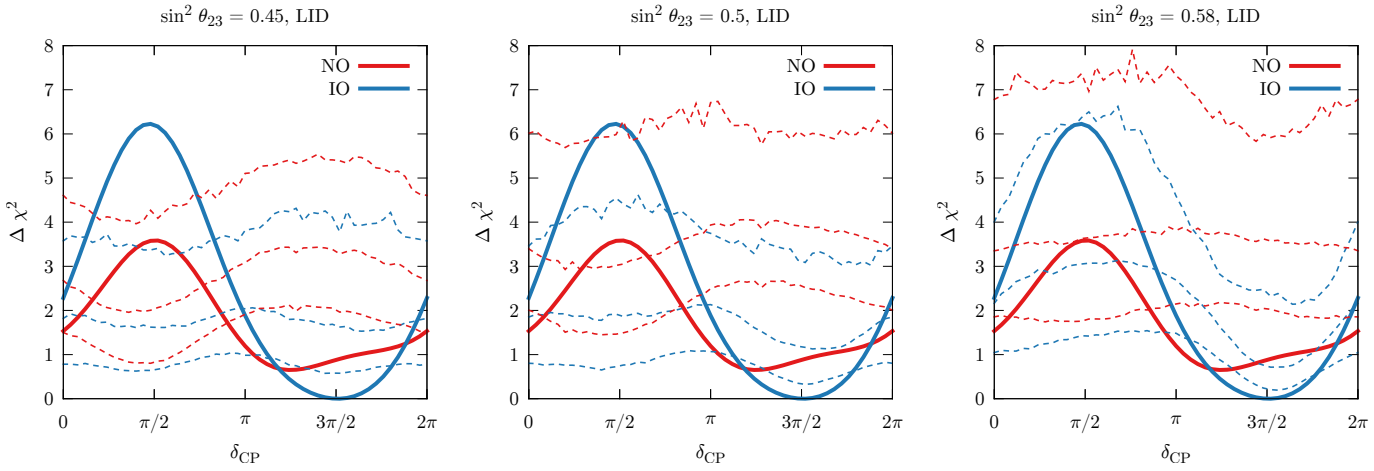

(c) NOνA, T2K and MINOS data

Figure 3.4: Experimental value of the test statistic (3.1) (solid) and its confidence levels (dashed) both for NO (red) and IO (blue) and different "true" θ_{23} values. The dashed lines correspond, from bottom to top, to 68.27%, 90% and 99% CL LID data. The discrete "steps" present in the NOνA CLs are due NOνA fitting a single Poisson-distributed discrete variable (the total number of ν_e events) therefore introducing a discretisation in the possible χ^2 values.

$\delta_{\rm CP}$ and ordering, that value of the phase can be excluded for that ordering with confidence λ. Conversely, if the real $\Delta\chi^2$ for a given ordering is larger than the values obtained for a fraction λ of the pseudo-experiments for that "true" mass ordering and any value of the "true" CP phase, the mass ordering is excluded with confidence λ. As has been mentioned previously, graphically this is equivalent to rejecting a value of $\delta_{\rm CP}$ and the mass ordering with a given CL if their experimental $\Delta\chi^2$ curve (solid line) is above the dashed line corresponding to that CL.

Getting to the results, regarding the mass ordering, from the panels in the centre line of Fig. 3.3 it can be read that the combination of NOνA LEM and T2K data discards IO with a 99% CL for almost all values of $\delta_{\rm CP}$ and for any of the three true values of θ_{23} considered. For $\delta_{\rm CP}$ around $\frac{3\pi}{2}$, IO is ruled out with a slightly lower CL but clearly larger than 90%. Adding MINOS data dilutes the significance of this disfavouring of IO: as seen in the lower panels of the figure, the region around $\delta_{\rm CP} \sim \frac{3\pi}{2}$ cannot be disfavoured even with 1 σ for any of the considered θ_{23} values. In particular, with MINOS data IO is disfavoured with a 99% CL only for $\delta_{\rm CP} \in [0.13\pi, 0.78\pi]$.

Regarding the allowed ranges of the CP phase, as shown in the figure, they are strongly dependent on the true value of θ_{23}. Also, for any value of θ_{23} the inclusion of MINOS dilutes the significance of leptonic CP violation. For example, the combination of NOνA+T2K+MINOS (for both LID and LEM) only disfavours CP conservation (i.e., $\delta_{\rm CP} = 0, 2\pi$) at about 1σ. Conversely, $\delta_{\rm CP} \in [0.16\pi, 0.84\pi]$ is disfavoured with a 90% C.L by NOνA LEM+T2K+MINOS for any value of true θ_{23}.

Chapter 4

Conclusions

This work is an introduction to research in the phenomenology of neutrino oscillations in the present experimental context. With this aim, a review of the theoretical and experimental status of neutrino oscillations has been first presented. In particular, the last data published by the NOνA collaboration has been analysed, their results replicated, and the information included in an updated global neutrino fit that is now public.

The NOνA experiment was especially designed for detecting electron neutrino appearance in a muon neutrino beam. It has been shown that this specific data, with just 7% of the total nominal exposure, already adds information on the three less-known neutrino oscillation parameters: the θ_{23} octant, δ_{CP} and the mass ordering. In particular, with LEM data $\theta_{23} > 45°$, $\delta_{\text{CP}} \sim \frac{3\pi}{2}$, and NO are now favoured.

In order to address our present knowledge of these parameters after including the NOνA results, a dedicated analysis has been carried out. This analysis quantifies the current statistical confidence on leptonic CP violation and the neutrino mass ordering taking into account possible deviations from Gaussianity via a MC simulation. It has included data from most modern accelerator neutrino experiment: NOνA, T2K and MINOS.

Quantitatively, at present CP conservation (i.e., $\delta_{\text{CP}} = 0, 2\pi$) is only disfavoured at about 1σ, while $\delta_{\text{CP}} \in [0.16\pi, 0.84\pi]$ is disfavoured with a 90% CL for any value of θ_{23}. Besides, the inverted ordering is disfavoured with a 90% CL for $\delta_{\text{CP}} \lesssim \pi$.

That information is significantly affected not only by individual uncertainties on the θ_{23} octant, δ_{CP} and the mass ordering, but also by the existing correlations between them. Therefore, as more data becomes available, global analyses could shed some light on these parameters. It is of particular importance the Neutrino 2016 Conference that will take place in early July 2016: NOνA data with twice as statistics and T2K antineutrino data with the same statistics as their neutrino data will be presented. After replicating the results of these experiments with a procedure similar to the one in this work, the combined analyses presented here, run on the new data, will lead to a publication.

The study of neutrino physics started with a brave proposal by Pauli of an almost undetectable particle. The combination of theoretical and experimental courage led to colossal detectors that undoubtedly determined that neutrinos have mass, thus providing a clear sign of new physics beyond the Standard Model. Currently, precision experiments are determining the last aspects of leptonic flavour mixing, guiding us towards a better understanding of Nature.

Acknowledgements

I would like to acknowledge several persons that have been fundamental to the development of this work. First, I want to thank my advisor, Concha Gonzalez-García, for her continuous support, advice, inspiring ideas, fruitful discussions, and vast knowledge of the field. I also feel grateful to the rest of the NuFIT group, in particular Michele Maltoni and Thomas Schwetz for fruitful discussions and ideas and for sharing the T2K and MINOS simulation code. Finally, I would also like to recognise the work of the NOνA collaboration and their supporting agencies for backing basic research on fundamental particle physics.

References

[1] I. Esteban, M. C. Gonzalez-Garcia, M. Maltoni, I. Martinez-Soler, and T. Schwetz, "NuFIT 2.1: Three-neutrino fit based on data available in May 2016", 2016. http://www.nu-fit.org/?q=node/115.

[2] W. Pauli, "Pauli letter collection: letter to Lise Meitner." Typed copy, Dec., 1930. http://cds.cern.ch/record/83282.

[3] M. C. Gonzalez-Garcia, M. Maltoni, and T. Schwetz, "Updated fit to three neutrino mixing: status of leptonic CP violation", *JHEP* **11** (2014) 052, arXiv:1409.5439 [hep-ph].

[4] M. Masud and P. Mehta, "Non-standard interactions spoiling the CP violation sensitivity at DUNE and other long baseline experiments", arXiv:1603.01380 [hep-ph].

[5] O. G. Miranda, M. Tortola, and J. W. F. Valle, "New ambiguity in probing CP violation in neutrino oscillations", arXiv:1604.05690 [hep-ph].

[6] LBNE Collaboration, C. Adams *et al.*, "The Long-Baseline Neutrino Experiment: Exploring Fundamental Symmetries of the Universe", arXiv:1307.7335 [hep-ex].

[7] Hyper-Kamiokande Collaboration, K. Abe *et al.*, "Physics potential of a long-baseline neutrino oscillation experiment using a J-PARC neutrino beam and Hyper-Kamiokande", *PTEP* **2015** (2015) 053C02, arXiv:1502.05199 [hep-ex].

[8] H. Bethe and R. Peierls, "The Neutrino", *Nature. Letters to the Editor* **133** (May, 1934) 689–690.

[9] C. L. Cowan, F. Reines, F. B. Harrison, H. W. Kruse, and A. D. McGuire, "Detection of the free neutrino: a confirmation", *Science* **124** no. 3212, (1956) 103–104.

[10] For the T2K Collaboration, M. Scott, "Recent results from T2K", in *30th Rencontres de Physique de La Vallée d'Aoste La Thuile, Aosta valley, Italy, March 6-12, 2016*. 2016. arXiv:1606.01217 [hep-ex].

[11] NOνA Collaboration, P. Adamson *et al.*, "First measurement of muon-neutrino disappearance in NOνA", *Phys. Rev.* **D93** no. 5, (2016) 051104, arXiv:1601.05037 [hep-ex].

[12] NOνA Collaboration, P. Adamson *et al.*, "First measurement of electron neutrino appearance in NOνA", *Phys. Rev. Lett.* **116** no. 15, (2016) 151806, arXiv:1601.05022 [hep-ex].

[13] For the MINOS Collaboration, L. H. Whitehead, "Neutrino Oscillations with MINOS and MINOS+", *Nucl. Phys.* **B908** (2016) 130–150, arXiv:1601.05233 [hep-ex].

[14] For the Daya Bay Collaboration, W. Tang, "Recent Results from the Daya Bay Neutrino Experiment", in *9th International Conference on Interconnections between Particle Physics and Cosmology (PPC2015) Deadwood, SD, USA, June 29-July 03, 2015*. 2015. arXiv:1512.00335 [hep-ex].

[15] For the Super-Kamiokande Collaboration, R. Wendell, "Atmospheric Results from Super-Kamiokande", *AIP Conf. Proc.* **1666** (2015) 100001, arXiv:1412.5234 [hep-ex].

[16] IceCube Collaboration, M. Aartsen *et al.*, "Determining neutrino oscillation parameters from atmospheric muon neutrino disappearance with three years of IceCube DeepCore data", *Phys. Rev.* **D91** no. 7, (2015) 072004, arXiv:1410.7227 [hep-ex].

[17] M. C. Gonzalez-Garcia and M. Maltoni, "Phenomenology with Massive Neutrinos", *Phys. Rept.* **460** (2008) 1–129, arXiv:0704.1800 [hep-ph].

[18] Particle Data Group Collaboration, K. A. Olive *et al.*, "Review of Particle Physics", *Chin. Phys.* **C38** (2014) 090001.

[19] V. Gribov and B. Pontecorvo, "Neutrino astronomy and lepton charge", *Physics Letters B* **28** no. 7, (1969) 493 – 496.

[20] B. A. Kniehl and A. Pilaftsis, "Mixing renormalization in Majorana neutrino theories", *Nucl. Phys.* **B474** (1996) 286–308, arXiv:hep-ph/9601390 [hep-ph].

[21] P. Ramond, "The Family Group in Grand Unified Theories", in *International Symposium on Fundamentals of Quantum Theory and Quantum Field Theory Palm Coast, Florida, February 25-March 2, 1979*, pp. 265–280. 1979. arXiv:hep-ph/9809459 [hep-ph].

[22] M. Gell-Mann, P. Ramond, and R. Slansky, "Complex Spinors and Unified Theories", in *Supergravity*, P. van Nieuwenhuizen and D. Freedman, eds., pp. 315–321. Amsterdam, North Holland, 1979. arXiv:1306.4669 [hep-th].

[23] T. Yanagida, "Horizontal gauge symmetry and masses of neutrinos", in *Proceedings of the Workshop on the Unified Theory and the Baryon Number in the Universe*, O. Sawada and A. Sugamoto, eds., vol. 79-18 of *KEK report*, pp. 95–98. 1979.

[24] R. N. Mohapatra and G. Senjanovic, "Neutrino Mass and Spontaneous Parity Violation", *Phys. Rev. Lett.* **44** (1980) 912.

[25] E. K. Akhmedov and A. Yu. Smirnov, "Paradoxes of neutrino oscillations", *Phys. Atom. Nucl.* **72** (2009) 1363–1381, arXiv:0905.1903 [hep-ph].

[26] L. Wolfenstein, "Neutrino Oscillations in Matter", *Phys. Rev.* **D17** (1978) 2369–2374.

[27] S. P. Mikheev and A. Yu. Smirnov, "Resonance Amplification of Oscillations in Matter and Spectroscopy of Solar Neutrinos", *Sov. J. Nucl. Phys.* **42** (1985) 913–917. [Yad. Fiz.42,1441(1985)].

[28] G. W. Gibbons, S. Gielen, C. N. Pope, and N. Turok, "Measures on Mixing Angles", *Phys. Rev.* **D79** (2009) 013009, arXiv:0810.4813 [hep-ph].

[29] S. F. King and C. Luhn, "Neutrino Mass and Mixing with Discrete Symmetry", *Rept. Prog. Phys.* **76** (2013) 056201, arXiv:1301.1340 [hep-ph].

[30] P. Huber, "On the determination of anti-neutrino spectra from nuclear reactors", *Phys. Rev.* **C84** (2011) 024617, arXiv:1106.0687 [hep-ph]. [Erratum: Phys. Rev.C85,029901(2012)].

[31] T. A. Mueller *et al.*, "Improved Predictions of Reactor Antineutrino Spectra", *Phys. Rev.* **C83** (2011) 054615, arXiv:1101.2663 [hep-ex].

[32] A. Palazzo, "Hint of non-standard dynamics in solar neutrino conversion", *Phys. Rev.* **D83** (2011) 101701, arXiv:1101.3875 [hep-ph].

[33] LSND Collaboration, A. Aguilar-Arevalo *et al.*, "Evidence for neutrino oscillations from the observation of anti-neutrino(electron) appearance in a anti-neutrino(muon) beam", *Phys. Rev.* **D64** (2001) 112007, arXiv:hep-ex/0104049 [hep-ex].

[34] C. Lujan-Peschard, G. Pagliaroli, and F. Vissani, "Counting muons to probe the neutrino mass spectrum", *Eur. Phys. J.* **C73** (2013) 2439, arXiv:1301.4577 [hep-ph].

[35] Super-Kamiokande Collaboration, S. Fukuda *et al.*, "Solar B-8 and hep neutrino measurements from 1258 days of Super-Kamiokande data", *Phys. Rev. Lett.* **86** (2001) 5651–5655, arXiv:hep-ex/0103032 [hep-ex].

[36] Borexino Collaboration, G. Ranucci *et al.*, "Overview and accomplishments of the Borexino experiment", *J. Phys. Conf. Ser.* **675** no. 1, (2016) 012036.

[37] SNO Collaboration, A. Bellerive, J. R. Klein, A. B. McDonald, A. J. Noble, and A. W. P. Poon, "The Sudbury Neutrino Observatory", *Nucl. Phys.* **B908** (2016) 30–51, arXiv:1602.02469 [nucl-ex].

[38] Double Chooz Collaboration, F. Ardellier *et al.*, "Letter of intent for Double-CHOOZ: A Search for the mixing angle theta(13)", arXiv:hep-ex/0405032 [hep-ex].

[39] RENO Collaboration, J. K. Ahn *et al.*, "RENO: An Experiment for Neutrino Oscillation Parameter θ_{13} Using Reactor Neutrinos at Yonggwang", arXiv:1003.1391 [hep-ex].

[40] A. Cervera, A. Donini, M. B. Gavela, J. J. Gomez Cadenas, P. Hernandez, O. Mena, and S. Rigolin, "Golden measurements at a neutrino factory", *Nucl. Phys.* **B579** (2000) 17–55, arXiv:hep-ph/0002108 [hep-ph]. [Erratum: Nucl. Phys.B593,731(2001)].

[41] A. Ghosh, T. Thakore, and S. Choubey, "Determining the Neutrino Mass Hierarchy with INO, T2K, NOνA and Reactor Experiments", *JHEP* **04** (2013) 009, arXiv:1212.1305 [hep-ph].

[42] S. K. Agarwalla, S. Prakash, and S. U. Sankar, "Resolving the octant of theta23 with T2K and NOνA", *JHEP* **07** (2013) 131, arXiv:1301.2574 [hep-ph].

[43] NOνA Collaboration, D. S. Ayres *et al.*, "NOνA: Proposal to build a 30 kiloton off-axis detector to study $\nu_\mu \to \nu_e$ oscillations in the NuMI beamline", arXiv:hep-ex/0503053 [hep-ex].

[44] NOνA Collaboration, D. S. Ayres *et al.*, "The NOνA Technical Design Report", Tech. Rep. FERMILAB-DESIGN-2007-01, Fermilab, 2007.

[45] For the NOνA Collaboration, R. B. Patterson, "First oscillation results from NOνA", in *Joint Experimental-Theoretical Seminar, Fermilab, August 6, 2015*. 2015. http://theory.fnal.gov/jetp/talks/20150806_nova_docdb.pdf.

[46] K. Sachdev, *Muon Neutrino to Electron Neutrino Oscillation in NOνA*. PhD thesis, University of Minnesota, Aug, 2015. http://lss.fnal.gov/archive/thesis/2000/fermilab-thesis-2015-20.pdf.

[47] C. Backhouse and R. B. Patterson, "Library Event Matching event classification algorithm for electron neutrino interactions in the NOνA detectors", *Nucl. Instrum. Meth.* **A778** (2015) 31–39, arXiv:1501.00968 [physics.ins-det].

[48] S. M. Lein, *Muon Neutrino Contained Disappearance in NOνA*. PhD thesis, University of Minnesota, Sep, 2015. https://inspirehep.net/record/1391606/files/fermilab-thesis-2015-21.pdf.

[49] S. S. Wilks, "The Large-Sample Distribution of the Likelihood Ratio for Testing Composite Hypotheses", *Annals Math. Statist.* **9** no. 1, (1938) 60–62.

[50] J. A. Formaggio and G. P. Zeller, "From eV to EeV: Neutrino Cross Sections Across Energy Scales", *Rev. Mod. Phys.* **84** (2012) 1307, arXiv:1305.7513 [hep-ex].

[51] S. G. Johnson, "Cubature (multi-dimensional integration)", 2010. http://ab-initio.mit.edu/wiki/index.php/Cubature. [Online; accessed 19-June-2016].

[52] F. James and M. Roos, "Minuit: A System for Function Minimization and Analysis of the Parameter Errors and Correlations", *Comput. Phys. Commun.* **10** (1975) 343–367.

[53] H. Nunokawa, S. J. Parke, and R. Zukanovich Funchal, "Another possible way to determine the neutrino mass hierarchy", *Phys. Rev.* **D72** (2005) 013009, arXiv:hep-ph/0503283 [hep-ph].

[54] For the NOvA Collaboration, J. Bian, "First Results of ν_e Appearance Analysis and Electron Neutrino Identification at NOvA", in *Proceedings, Meeting of the APS Division of Particles and Fields (DPF 2015)*. 2015. arXiv:1510.05708 [hep-ex].

[55] J. Elevant and T. Schwetz, "On the determination of the leptonic CP phase", *JHEP* **09** (2015) 016, arXiv:1506.07685 [hep-ph].